

Investigation on the opportunity to introduce prognostic techniques in railway axles maintenance

Mattia Vismara¹

¹*Hupac SA, Chiasso, Switzerland*
mvismara@hupac.ch

ABSTRACT

In this study the opportunity to introduce PHM (prognostic and health monitoring) concepts into a cracked railway axle management is investigated.

The performances of two different prognostic algorithm are assessed on the basis of their RUL (remaining useful life) predictions accuracy: a prognostic model based on the Bayesian theory and a physical prognostic model. Both models rely on the measured crack size. The measured crack growth measure has been built from simulated probabilistic crack growth path by adding measurements errors. The effect of monitoring frequency and the measurement HW and SW infrastructure size error to RUL predictions' accuracy is assessed as well, trying to evaluate the hypothetical measuring infrastructure capabilities' (sensors + layout) effect on the overall PHM predictions.

Furthermore the PHM approach is compared to the classical preventive maintenance approach to railway axle maintenance management based on expensive and regular NDT.

1. INTRODUCTION

Railway axles are designed to have an infinite lifetime (EN13103, 2001). However occasional failures have been and are observed in service. The typical failure positions are the press-fits for wheels, gears, and brakes or the axle body close to notches and transitions. Such failures always occur as fatigue crack propagations whose nucleation can be due to different causes (U. Zerbst M. V., 2005). In the case of railway axles, the presence of widespread corrosion (Hoddinot, 2004) (C.P. Lonsdale, 2004) or the possible damage due to the ballast impacts (M. Carboni, 2007) may constitute such causes.

This kind of failures is usually tackled by employing the 'damage tolerance' methodology, whose philosophy consists (U. Zerbst M. V., 2005) (U. Zerbst K. M., 2005) in determining the most opportune inspection interval given the 'probability of detection' (PoD) of the adopted non-

destructive testing (NDT) technique or, alternatively, in defining the needed NDT specifications given a programmed inspection interval.

The negligible number of axle failures is reached thanks to role played by inspections carried out with the aim of keeping developing fatigue problems at bay. As reported by (R.A. Smith, 2004) in the United Kingdom there have been about 1.6 axle failures per year over the last 25 years, out of a population of about 180,000 axles. (A similar number of new axles are introduced every year in PR China, where some 2.5×10^6 wheelsets are in fleet service.) These large numbers of axles are subjected to inspections in order to try to identify cracks before failures occur. In general, the examinations are expensive, time consuming and not particularly effective in finding cracks. Furthermore, the dismantling needed to examine axles, such as the drawing-off of bearings, can cause scratching damage that is sufficiently severe to cause an axle to be retired. The rationale behind the frequency of testing is that the largest crack that would not be detected in an inspection should not grow to failure during the service interval to the next inspection. This implies that crack propagation calculations should be performed with sufficient accuracy to set the inspection interval. However, as stated by (R.A. Smith, 2004) some difficulties arises:

- Due to the difficulty in determining the reliability and sensitivity of the inspection techniques, the initial crack length chosen for the life calculation must be set larger, leading to shorter intervals between inspections than are really necessary.
- The service loads are much more stochastic in nature than the well-defined hypothetical loads used for the initial design rule suggest. In many cases, in the absence of experimental measurement, the magnitudes and frequencies of these events are unknown, thus making cycle-by-cycle crack growth predictions unreliable.
- Important inputs to fatigue calculations are material properties such as crack growth data, fatigue limits and fatigue thresholds, which are very sensitive to material condition, manufacturing route, surface treatment, orientation and load sequence. In many cases these data

M.Vismara. This is an open-access article distributed under the terms of the Creative Commons Attribution 3.0 Unported License, which permits unrestricted use, distribution, and reproduction in any medium, provided the original author and source are credited.

are lacking, particularly from large specimens representative of axles.

- Abnormal conditions may arise in service. There is debate about the best means of protecting axles from corrosion and the extent to which coatings may hinder inspection. The interactions between fatigue and corrosion mechanisms in extending defects are still inadequately understood. Higher speeds have led to increased examples of damage of axles from flying ballast, which may be of the form of crack-like indentations on axle surfaces that initiate premature failure.

These considerations can lead to think that maybe, instead of using a preventive maintenance approach a predictive maintenance approach based on prognostics could be convenient. Several aspects has to be considered in order to assess the technical and economical feasibility of this approach. The first and the most important is the assessment of the prognostic algorithm predictions accuracy and its sensibility to the goodness of the diagnostic and monitoring equipment used.

This section constitute the first attempt to answer to this question through an explanatory assessment of two prognostic algorithms. The first one is based on statistical method, the second one exploit the good understanding of the crack propagation physical process to estimate the time to fail of a cracked axle. Moreover, the predictive maintenance approach is qualitatively compared to the classical preventive approach.

2. PROBLEM FORMULATION

2.1 Simulation of the crack growth paths – The stochastic crack growth algorithm

In this paragraph the stochastic crack growth model used in this work is presented. The non-powered railway axle considered in the present study is manufactured in A1N steel and used in Y25 bogie with a diameter D equal to 160 mm.

Service loads acting on railway axles are the result of vertical and lateral forces (EN13103, 2001) due to their normal functioning, and the maximum bending moments can be found in the area of the wheels press-fit (U. Zerbst M. V., 2005)(M. Carboni, 2007). On the basis of these considerations, fatigue crack growth has here been analyzed at the typical T-transition between the axle body and the press-fits.

Different algorithms for simulating the crack growth of cracked components are available in literature. Some of them consider the crack growth modeling as stochastic process, see for example (K.Ortiza, 1988),(D.A. Virkler, 1979),(J.L Bogdanoff, 1985). However, the likelihood of lifetime calculations depends on the adopted FCG algorithm

and only the most complex algorithms are able to adequately describe crack propagation under variable amplitude loading in railway axles (S. Beretta M. C., 2006).

In the present work the NASGRO algorithm (Anonymus, 2006) will be considered. This FCG model has been chosen because it is the reference algorithms in analyses where random loadings are involved, since it takes into account the “plasticity-induced crack closure” phenomenon (EN13103, 2001). Moreover, NASGRO has been used in several papers addressing the propagation of fractures in railway axles (U. Zerbst M. V., 2005) (S.Beretta M. , Simulation of fatigue crack propagation in railway axles, 2005)(S. Beretta M. C., 2004).

The considered software adopts the Paris-based crack propagation law called “NASGRO equation”:

$$\frac{da}{dN} = C \left[\left(\frac{1-f}{1-R} \right) \Delta K \right]^n \frac{\left(1 - \frac{\Delta K_{th}}{\Delta K} \right)^p}{\left(1 - \frac{\Delta K}{(1-R)\Delta K_{crit}} \right)^q} \quad 2.1$$

where “C”, “n”, “p” and “q” are empirical constants, “R” is the stress ratio, “ ΔK_{th} ” is the threshold SIF range and “ ΔK_{crit} ” the critical SIF.

To analyze cracked bodies under combined loading, the stress intensity factor is expressed as:

$$\Delta K_{nom} = \left[\sum_{i=1}^6 \alpha_i \left(\frac{a}{D} \right)^i + \beta \right] (1-R)(S+\varepsilon)\sqrt{\pi a} \quad 2.2$$

Where α_i and β are empirical constants, S is the applied bending stress, a is the crack size and ε is a random coefficient (introduced later in the paragraph). The bending stress is considered plane since NASGRO is not able to consider rotating bending conditions. This assumption has not a significant influence on estimated life predictions as demonstrated in (S.Beretta M. , Rotating vs. plane bending for crack growth in railway axles, 2005)(S.Beretta M. M., 2006).

The closure function is defined as:

$$f = A_0 + A_1 R \quad 2.3$$

Where

$$A_0 = 0.825 - 0.34\vartheta + 0.05\vartheta^2 \left[\cos\left(\frac{\pi}{2}S_0\right) \right]^{\frac{1}{\vartheta}} \quad 2.4$$

$$A_1 = (0.415 - 0.071\vartheta)S_0$$

ϑ is a plane stress/strain constraint and S_0 is the ratio of the maximum applied stress to the flow stress.

Since NASGRO does not consider the geometry of the typical transitions of axles, equation 2.5 is modified in terms of the maximum SIF present at the notch root and calculated as

$$\Delta K = K_t \Delta K_{nom} \quad 2.6$$

K_t represents the experimental stress concentration (S. Beretta M. C., 2004).

As demonstrated by (S. Beretta M. C., 2006), the crack growth randomness can be described considering the stress intensity factor threshold as a random variable. Particularly, it is demonstrated that ΔK_{th} can be considered as belonging indifferently to a lognormal distribution or normal distribution. In this work is considered as a normal variable with mean ΔK_{th} and standard deviation $\sigma_{\Delta K_{th}}$. The empirical calibration of all the other parameters is carried out by means of dedicated fracture mechanic experiments. Their values are listed in Appendix. Another relevant source of uncertainty is the randomness of the applied load (U. Zerbst M. V., 2005)(M. Carboni, 2007). Therefore service loads have been considered derived from experimental results on a high speed train. Next, the service stress spectrum has been approximated with a simple block loading consisting of twelve blocks (Table 1). To take into account the within block variability a random term ε is added in the Eq.2.9. It is assumed to be uniformly distributed with mean equal to 0 and with a span of 2ε .

The so defined block loadings were then applied to growth calculations with a time sequence in accordance to Gassner suggestions (Gassner, 1956). Starting from the discrete spectrum in Table 1, the random history loads sequence is built by permutations of the whole set of the blocks. Each load sequence is 3.222.887 km long, composed of 20 consecutive complete permutations. Some simulated crack growth path, considering all the uncertainties described (load history, ΔK_{th} and ε) are shown in Figure 1.

Cycles	Load [MPa]
1	145
8	135
75	125
825	115
15,000	105
110,025	95
357,675	85
678,900	75
1,621,725	65
3,046,500	55
8,165,775	45

39,718,275 35

Table 1 The 12 service time blocks

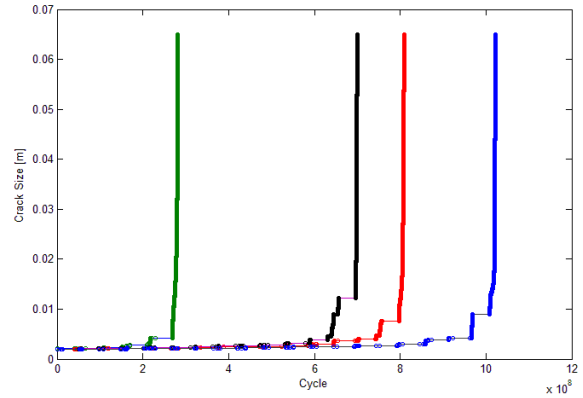


Figure 1 Examples of simulated crack growth paths

Eventually, once determined an initial crack size and a limiting crack depth value at failure, through the Monte Carlo technique is possible to estimate the TTF pdf. Each simulation run is characterized by a random ΔK_{th} and a random load history. Considering an initial crack size of 2 mm and a limiting crack size of 60 mm, the TTF pdf is shown in Figure 2.

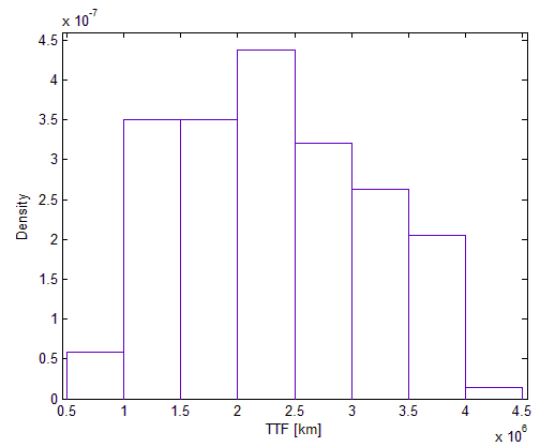


Figure 2 TTF probability distribution

The TTF pdf for the purposes of this work is considered as a lognormal distribution as can be observed in Figure 3. It can be noticed how a lognormal distribution fits well the TTF data for almost the whole TTF variability range, only the right hand tail significantly diverge for the TTF. This is demonstrated also by Beretta et al. (S. Beretta M. C., 2006) and Schijve (Schijve, 2001).

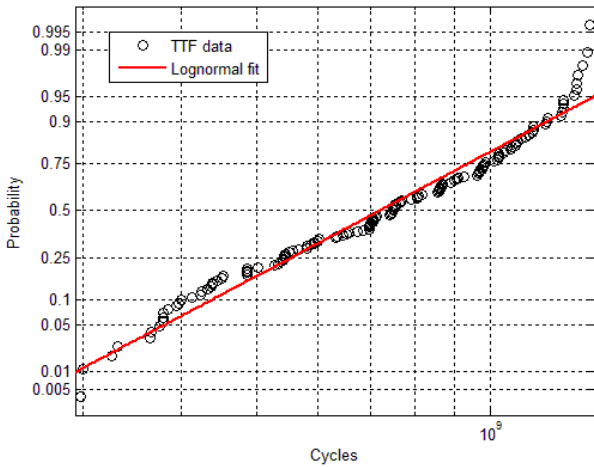


Figure 3 Lognormal fit plot for TTF pdf

2.2 Design of the preventive maintenance approach

The preventive maintenance approach is designed according to the damage tolerant approach well described by (U. Zerst M. V., 2005) (U. Zerst K. M., 2005). The steps that have to be followed to design a design an axle preventive maintenance plan are:

1. establishment of the initial crack shape and size for further analysis
2. within a damage tolerance concept the initial crack size, a_0 , is not identical to the size of a real flaw, e.g., from the manufacturing process but is a fictitious size, which usually refers to the detection limit of the NDI technique. The basic idea is that the largest crack that could escape detection is presupposed as existent.
3. simulation of sub-critical crack extension, This kind of crack growth is designated as sub-critical since it will not lead to immediate failure until a critical length of the crack is reached. For railway applications the common mechanism is fatigue.
4. determination of critical crack size for component failure. The sub-critical crack extension is terminated by the failure of the component. This may occur as brittle fracture or as unstable ductile fracture. Critical states may, however, also be defined by other events such as stable ductile crack initiation or the break-through of a surface crack through the wall or setting a maximum allowable crack size threshold.
5. determination of residual lifetime of the component, The residual lifetime is that time or number of loading cycles which a crack needs for extending from the initial crack size, a_0 , (step 1) up to the allowable crack size, a_{max} , established in step (3).
6. specification of requirements for non-destructive testing.

The constitution of an inspection plan is the aim of a damage tolerance analysis. From the requirement that a potential defect must be detected before it reaches its critical size it follows immediately that the time interval between two inspections has to be smaller than the residual lifetime. Sometimes inspection intervals are chosen to be smaller than half this time span. The idea is to have a second chance for detecting the crack prior to failure if it is missed in the first inspection. It is, however, also obvious that frequently even two or more inspections cannot guarantee the crack being detected since this would require a 100% probability of detection.

The procedure described by (U. Zerst M. V., 2005) aims to define the NDT specifications following the 'last chance' approach introduce in (M. Carboni, 2007). In this case, the PoD is not a variable to be optimized but is given. Therefore the maximum inspection interval was defined instead of the requirements for non destructive testing. The steps from 1 to 4 has already been done in the previous paragraph.

2.2.1 The PoD curve

The PoD can be derived from the calibration function of the particular NDE equipment used that relates the crack dimension (length, depth or area) to the output. In this case, the NDE method considered is the ultrasonic inspection. Since output from an NDE measurement process is a continuous response, the calibration curve is modeled as a linear function in which the measurement (dB of the signal) is given by a linear combination of two parameters and the crack area (\hat{a} [mm^2]) plus a normal zero mean error with constant variance (Eq.2.7).

$$Y(\hat{a}) = \beta_0 + \beta_1 \log_{10} \hat{a} + \epsilon(0, \sigma_r) \quad 2.7$$

The parameters $\beta_0, \beta_1, \sigma_r$ are estimated through the LSE or through the MLE methods. Is assumed that 1000 dB and -1000dB are respectively the saturation and observable limits.

The data provided from which the parameters are estimated have been obtained from real inspections of railway axles. The parameters' values are reported in Table 2.

Parameter	Value*
β_0	Xxo
β_1	Yyo
σ_r	Zzo

Table 2: Calibration Curve Parameters

In order to use the calibration curve in the following analysis, the crack size has to be expressed in term on depth instead of surface area. The crack geometry is assumed to

* Values are omitted for confidentiality reasons

be semicircular (M. Carboni, 2007). Therefore, the resulting calibration curve function becomes:

$$Y = \beta_0 + \beta_1 \log_{10} \left(\frac{\pi a^2}{2} \right) + \epsilon (0, \sigma_r) \quad 2.8$$

In order to derive the PoD function, a threshold is fixed that represents the measure's bound that if it's overcome, the presence of a crack is diagnosed. This limit is set at 50.6 dB that corresponds to a crack depth of 5.492 mm.

The reference limit and the final calibration curve with the constant $3\sigma_r$ confidence limits is shown in Figure 4.

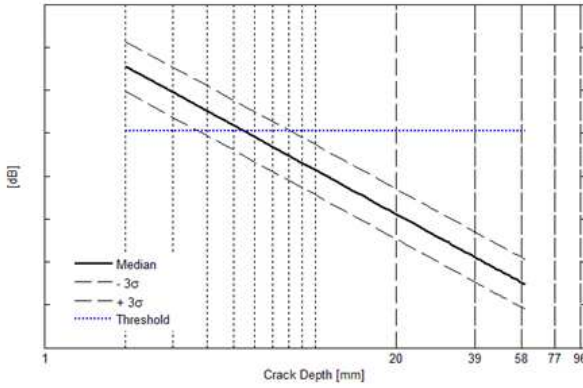


Figure 4: Final Calibration Curve

At this point the PoD curve can be derived as it represents the probability that a crack of size a can be detected, given that the threshold is set at a_{th} . According to this statement and making the hypothesis of a normal distributed error, the PoD of a crack depth a is:

$$\begin{aligned} PoD(a) &= P[Y(a) > Y(a_{th})] = \\ &= 1 - \Phi \left(\frac{Y(a_{th}) - \left(\beta_0 + \beta_1 \log_{10} \left(\frac{\pi a^2}{2} \right) \right)}{\sigma_r} \right) \quad 2.9 \\ &= 1 - \Phi \left(\frac{50.6 - \left(\beta_0 + \beta_1 \log_{10} \left(\frac{\pi a^2}{2} \right) \right)}{\sigma_r} \right) \end{aligned}$$

where Φ is the standard normal cdf. In Figure 5 is shown the resulting PoD curve.

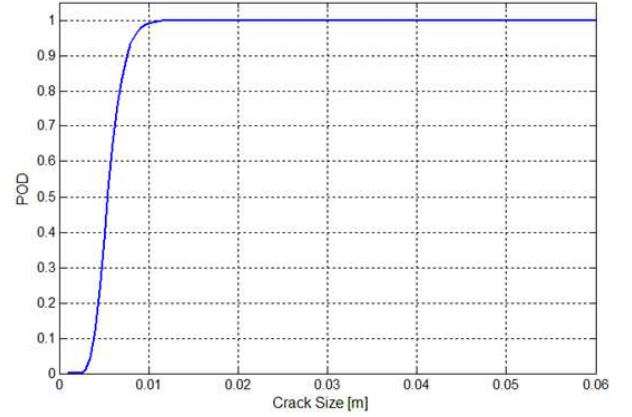


Figure 5: PoD

The PoD as discussed above in paragraph 2.2 is used to determine the maximum inspection interval in order to detect with a probability R the maximum allowed crack size a_{max} . In the following paragraph, according to the problem defined in paragraph 2.2, the maximum inspection interval is determined.

2.2.2 Identification of the maximum inspection interval

The maximum safe inspection interval is determined through examining the effect of the interval of inspection on the overall probability of detection in the case of a fast growing crack. The inspection interval is therefore the maximum interval of inspection that allows the detection of the maximum allowable crack size with a defined reliability. The worst case is when the time (or distance) before the failure occurs (TTF) is minimum. This happens when, once the maximum defect present in the system is set, the crack growth rate is the highest. The inspection interval is therefore dependent on the largest defect present in the system, that is the defect that will eventually cause failure.

The maximum defect size is set at 2 mm as suggested by the literature reviewed (M. Carboni, 2007) (U. Zerbst M. V., 2005) and as set in the crack growth simulations. At this point the fastest growth crack has to be chosen as the reference upon which the maximum allowable inspection interval has to be defined.

Starting from the TTF distribution shown in Figure 2, the fastest growth crack has been chosen. It is the crack growth path with the minimum TTF in 300 simulations and that falls in the first bin of the TTF distribution. In Figure 6 is shown the path selected and its relative position with respect to the TTF distribution (blue line). As can be seen it falls in the left tail of TTF pdf.

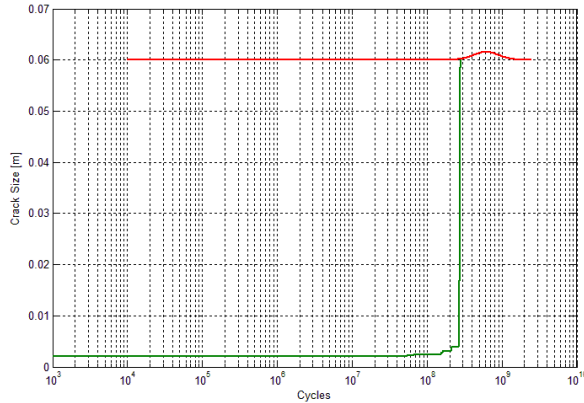


Figure 6 Fastest growth crack

Once the worst case is chosen and the reference PoD has been defined, the maximum inspection interval can be found.

Given an inspection interval, ‘I’, the cumulative PoD PC_{DET} of a defect, potentially observable in a given number of inspections, i , is calculated from the PoD curve of the adopted NDT technique. Figure 7 shows how the cumulative probability of detection is calculated, that in formulae results.

$$PC_{DET} = 1 - \prod_{i=1}^n PonD_i \quad 2.10$$

$$PonD_i = 1 - Pod_i$$

Here, PC_{DET} is the theoretical cumulative PoD and $PonD$ (‘probability of non-detection’) represents the probability of failing to detect in a given inspection.

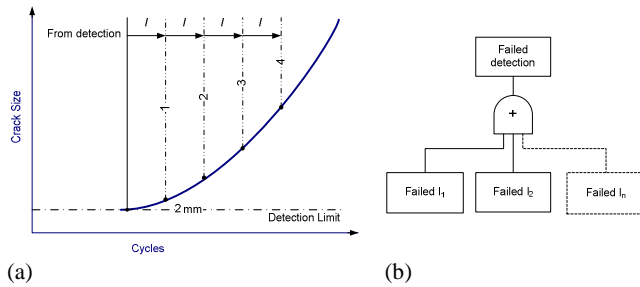


Figure 7 Calculation of the cumulative probability of detection (a) and the fault tree of the inspection (b) (adopted from (M. Carboni, 2007))

The PoD_i depends on the actual crack size a that corresponds to the cycle i according to the Eq. 2.9. The more the inspections the more the PC_{DET} will be.

Since a 100% PC_{DET} is impossible to reach theoretically, a PC_{DET} threshold was set at 0.99.

In order to determine the inspection interval the final PC_{DET} is evaluated at different intervals of inspection. Particularly, the final PC_{DET} was evaluated starting from 1 to 60 inspections that result in the same number of intervals.

The final PC_{DET} is the P_{DET} that results from the last inspection. Figure 8 shows the results of the assessment, it shows the PC_{DET} as a function of the inspection interval. The figure confirm what stated previously: as the number of inspection increases and the inspection interval decreases PC_{DET} increases. The optimal inspection interval is the largest that guarantee a $PC_{DET} = 0.99$.

From Table 3, can be seen that the inspection interval at 0.99 falls between 34,988 km and 32,297 km. By linear interpolation we can find that the interval at 99% PC_{DET} is **33,663 km**.

N° inspections	Inspection Interval [km]	PC_{DET}
1	419,856	0.000000
3	209,928	0.000014
5	139,952	0.003680
7	104,964	0.003694
9	83,971	0.007346
11	69,976	0.007360
13	59,979	0.010992
15	52,482	0.011006
17	46,651	0.026369
19	41,986	0.026967
21	38,169	0.397817
23	34,988	0.834808
25	32,297	0.999981

Table 3 PC_{DET} with different inspection interval

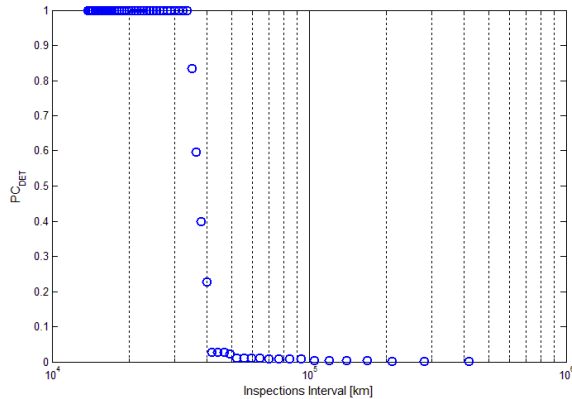


Figure 8 PC_{DET} as function of the inspection intervals

The literature reviewed (U. Zerbst M. V., 2005)(M. Carboni, 2007) (S. Beretta M. C., 2006) suggests to determine the inspection intervals referring to the average crack growth path, i.e whose TTF is equal to the mean TTF. In this case, once selected the right crack propagation lifetime, the maximum inspection interval is computed as well. The result is that the optimal inspection interval should be performed each 153,197.8 km. It is worth noting that in case of the fast crack growth crack, with an inspection interval equal to **153,197.8** km the PC_{DET} is equal to 0.2986%.

2.3 Prognostic Modeling of the Crack Size Growth

In this section two methods able to predict the RUL of cracked railway axles are introduced and compared in term of their prediction performances.

The first model uses a statistical approach based on the Bayesian probabilistic theory and the second one uses the physical model introduced in the paragraph 2.1, the same used to generate the crack growth paths. Since the model accurately describe the real crack growth in railway axles(S. Beretta M. C., 2006), it can be used both to substitute experimental tests and to generate the database needed to support a statistical approach to evaluate the axles' TTF and RUL.

The aim of the section is to introduce and give evidence of the capability of a prognostic approach based on these algorithms to reduce the uncertainties associated to the prediction of the TTF of a continuously monitored cracked axle meanwhile it operates. This approach can be helpful to increase the inspection interval and, as a best result, inspects the axle only when the wheels have to be maintained without reducing the system's safety.

2.3.1 Setting the threshold

In order to design a prognostic algorithm capable of updating the axle's TTF the concept of failure has to be

clearly determined. In this case it is trivially derived since the axle is considered faulty when the maximum allowable crack size is reached. Obviously, the threshold has to fixed considering the errors that affects the whole monitoring and prognostic system. Figure 10 shows a scheme of the different types of errors that has to be considered in setting the threshold. A safety margin has to be introduced against the errors that affect the estimation. The first error was introduced in the paragraph 2.2.1.

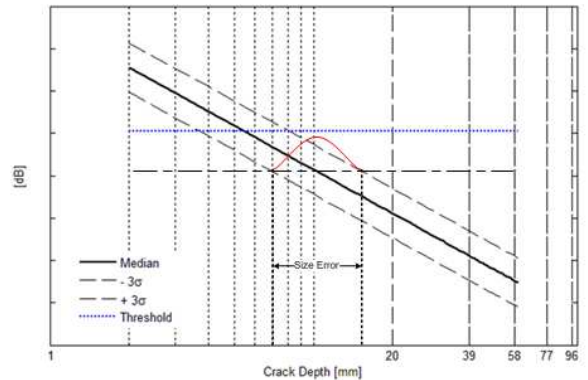


Figure 9 Illustration of the meaning of the size error

It is the error associated with the calibration curve of the ultrasonic inspection. This error introduces an uncertainty in the determination of the crack size given that the ultrasonic probe measures x dB.

Figure 9 illustrates what is meant for the size error. Given the calibration curve in Eq.2.8, the size error ϵ_s is defined as:

$$\epsilon_s = \frac{\epsilon}{\beta_1} \tag{2.11}$$

$$\epsilon_s = N\left(0, \frac{\sigma_r}{\beta_1}\right)$$

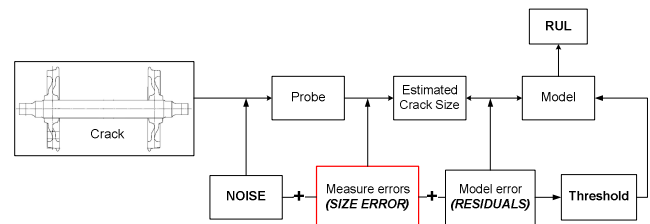


Figure 10 The errors affecting the monitoring and prognostic system

The other errors that are present are those associated with the model describing the crack growth, that are the residuals between the actual crack size and the that one predicted by the model and eventually the noise that affects the measurements process.

In this case the size error is only considered since no data are available about the other error sources. The error considered can be considered as the sum of those making the hypothesis that the used diagnostic system's performances are better.

Given a crack depth a_{max} as the maximum crack size allowed, the threshold that will be used as a reference for estimating the axle TTF is that one that guarantees at 99% of confidence that a_{max} won't be missed.

Starting from the calibration function in Eq.2.8 we have to find \tilde{a}_{th} that corresponds to $P(a_{max} \leq \tilde{a}_{th}) = 0.99$.

Starting from Eq.2.9, given the measure Y , the related crack size is:

$$a = \sqrt{\frac{2}{\pi} 10^{\frac{Y-\beta_0}{\beta_1}} 10^{\frac{\varepsilon}{2\beta_1}}} \quad 2.12$$

Remembering that $\varepsilon_s = \frac{\varepsilon}{\beta_1}$, we have:

$$a = \sqrt{\frac{2}{\pi} 10^{\frac{Y-\beta_0}{\beta_1}} 10^{\varepsilon_s}} \quad 2.13$$

Given that \hat{Y} corresponds to the measurement of the crack size a_{max} , we have:

$$a_{max} = \sqrt{\frac{2}{\pi} 10^{\frac{\hat{Y}-\beta_0}{\beta_1}} 10^{\varepsilon_s}} \quad 2.14$$

The crack size that corresponds to the measurement \hat{Y} is:

$$c \quad a = \sqrt{\frac{2}{\pi} 10^{\frac{\hat{Y}-\beta_0}{\beta_1}} 10^{\varepsilon_s}} \quad 2.15$$

$$a = a_{max} 10^{\frac{\varepsilon_s}{2}}$$

From Eq.2.15 we have that given a real crack depth of a_{max} the crack size associated a (estimated from the measurement) is a random variable distributed as a lognormal with an associated mean of $\log_{10}(a_{max})$ and a standard deviation of $\frac{\sigma_r}{2\beta_1}$.

$$\log_{10} a = \log_{10} \left(a_{max} 10^{\frac{\varepsilon_s}{2}} \right)$$

$$\log_{10} a = \log_{10}(a_{max}) + \log_{10} \frac{\varepsilon_s}{2} \quad 2.16$$

$$\log_{10} \frac{\varepsilon_s}{2} = N \left(0, \frac{\sigma_r}{2\beta_1} \right)$$

Now we can define the threshold \tilde{a}_{th} :

$$P(\tilde{a}_{th} - a_{max} \leq 0) \geq 0.99$$

$$\Phi \left(\frac{\log_{10} \tilde{a}_{th} - \log_{10} a_{max}}{\frac{\sigma_r}{2\beta_1}} \right) \geq 1 - 0.99 \quad 2.17$$

The result is $\tilde{a}_{th} = \mathbf{0.044}$.

If we let vary both σ_r and a_{max} and calculate the corresponding \tilde{a}_{th} we obtain a surface plotted in Figure 11. As we can see the relation is not linear and as the standard error increases, given a maximum crack size, the corresponding crack depth threshold decreases.

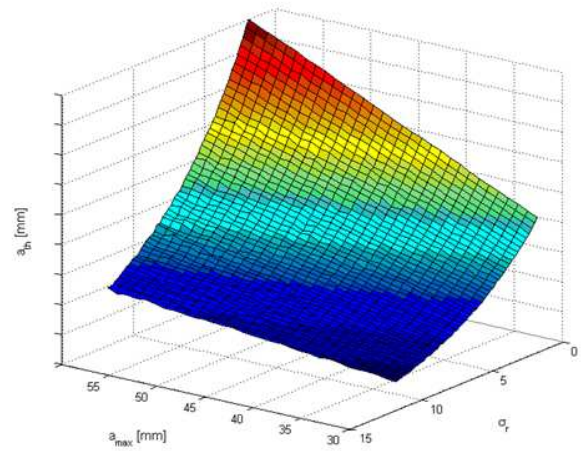


Figure 11 Crack size threshold as a function of σ_r and a_{max}

2.3.2 Bayesian updating algorithm

This section develops methods that combine two sources of information, the reliability characteristics of a axle's population and real-time sensor information from a functioning axle, to periodically update the distribution of the axles's residual life.

We first model the degradation signal for a population of axles with an appropriate model assuming error terms from an iid random error process. A Bayesian updating method is used to estimate the unknown stochastic parameters of the model for an individual component. Once we have determined the posterior distribution for these unknown parameters, we derive the residual-life distribution for the individual component.

In this case there is not simple functional form that fit well the simulated crack growth pattern. Nevertheless, an approximation of the paths can be performed by splitting the signal in two parts, that can be modeled as two exponential functions as shown in Figure 12.

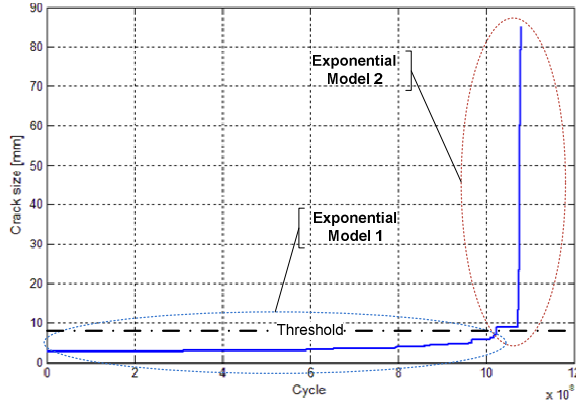


Figure 12 The two exponential models

The shift from the first model to the second is based on a crack depth threshold that is plotted in Figure 12 as a black dash dotted line. The TTF of the axle monitored is therefore defined as:

$$TTF = T_1 + T_2 \quad 2.18$$

Where T_1 is a random variable that express the predicted time to reach the threshold \tilde{S}_{th} and T_2 is a random variable as well that denote the time that takes the crack to grow from the threshold to \tilde{a}_{th} .

Let $S(t)$ denote the degradation signal as a continuous stochastic process, continuous with respect to cycle n . We observe the degradation signal at some discrete points in cycles, n_1, n_2, \dots , where $n_i \geq 0$. Therefore, we can model the degradation signal at cycles $n_i = n_1, n_2, \dots$, as follows:

$$\begin{cases} S(n_i) = \varphi_1 + \theta_1 \exp[\beta_1 n_i + \epsilon_1] & S \leq \tilde{S}_{th} \\ S(n_i) = \varphi_2 + \theta_2 \exp[\beta_2 n_i + \epsilon_2] & \tilde{S}_{th} \leq S \leq \tilde{a}_{th} \end{cases} \quad 2.19$$

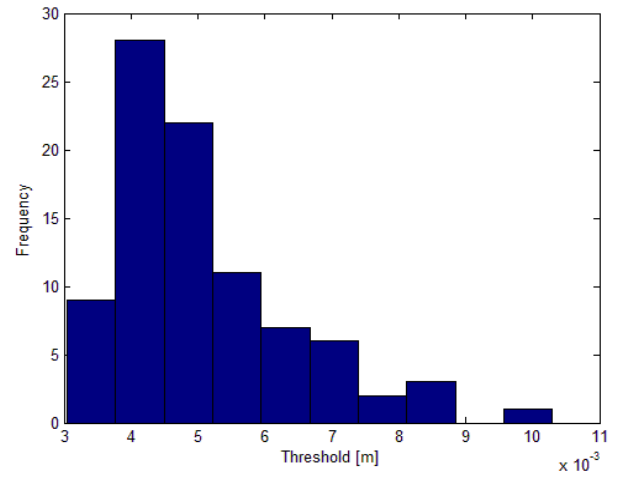
If we redefine $L_1(n_i) = S(n_i) - \varphi_1$ for $S \leq \tilde{S}_{th}$ and $L_2(n_i) = S(n_i) - \varphi_2$ for $\tilde{S}_{th} \leq S \leq \tilde{a}_{th}$ we obtain:

$$\begin{cases} L_1(n_i) = \theta_1 \exp[\beta_1 n_i + \epsilon_1(n_i)] & S \leq \tilde{S}_{th} \\ L_2(n_i) = \theta_2 \exp[\beta_2 n_i + \epsilon_2(n_i)] & \tilde{S}_{th} \leq S \leq \tilde{a}_{th} \end{cases} \quad 2.20$$

The choice of threshold \tilde{S}_{th} has to be based on an optimization rule. In this case, the threshold is that one that bound the maximum residual of the first fitted model to 0.0012. Obviously the rule can be changed, for example the threshold could be that one that minimize the overall fitting error. The value 0.0012 at which the first residual error is

bounded is chosen upon that willingness to prefer a better fit in the first part of the signal in order to achieve better predictions in the first stage of the degradation process. The reason is that good predictions (more precise) in the first part of the degradation path can restrict the uncertainties on the final RUL estimation from the beginning. As matter of facts, the main part of the uncertainty on the TTF comes from the uncertainty associated with the variable T_1 . In other words, the variance of the cycles taken by the crack to grow from the initial size to \tilde{S}_{th} is much greater that the number of cycles taken by the crack to grow from \tilde{S}_{th} to \tilde{a}_{th} .

After several simulations, the threshold that bound the maximum residual error of the first part of S is a random variable as shown in Figure 13.


 Figure 13 Threshold \tilde{S}_{th} distribution

Eventually the final threshold chosen is the mean value of distribution, that is $\tilde{S}_{th} = 5,1 \text{ mm}$.

Once determined the threshold, through an appropriate number of crack growth simulations, we can build our a priori information on the crack growth behavior. Our a priori information, a part from the a priori TTF distribution shown in Figure 2, is composed of the random parameters $\theta_1, \theta_2, \beta_1$ and β_2 probability distributions. Their values are obtained through the LSE technique though fitting the crack growth functions with the models in Eq.2.19. The final distribution PDFs are plotted in Figure 14.

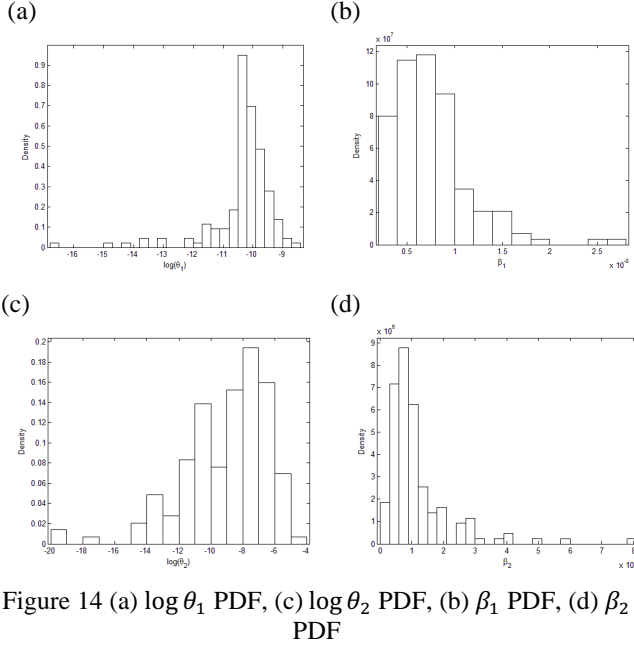


Figure 14 (a) $\log \theta_1$ PDF, (c) $\log \theta_2$ PDF, (b) β_1 PDF, (d) β_2 PDF

As can be noted from the figure above, $\theta_1, \theta_2, \beta_1$ and β_2 can be approximated by lognormal distributions[†] with parameters:

$$\begin{aligned} \theta_1 &= LN(\mu_{\theta_1}, \sigma_{\theta_1}) & \theta_2 &= LN(\mu_{\theta_2}, \sigma_{\theta_2}) \\ \beta_1 &= LN(\mu_{\beta_1}, \sigma_{\beta_1}) & \beta_2 &= LN(\mu_{\beta_2}, \sigma_{\beta_2}) \end{aligned}$$

The probability charts of those distributions can be found in the Appendix.

For these exponential models, it will be convenient to work with the logged signal S . We can then define the logged signal at cycle n_i as follows:

$$\begin{cases} LS_1(n_i) = \log \theta_1 + \beta_1 n_i + \epsilon_1(n_i) & c \leq \tilde{s}_{th} \\ LS_2(n_i) = \log \theta_2 + \beta_2 n_i + \epsilon_2(n_i) & \tilde{s}_{th} \leq S \leq \tilde{a}_{th} \end{cases} \quad 2.21$$

We will use the observations $LS_{i,1}, LS_{i,2}^{\ddagger}, \dots$, obtained at cycles n_1, n_2, \dots , as our data. Next, suppose we have observed $LS_{i,1}, \dots, LS_{i,k}$ at cycles n_1, \dots, n_k .

Since the error terms, $\epsilon_i(n_t)$, $i = 1, 2$ and $t = 1, \dots, k$, are assumed to be iid normal random variables, if we know $\theta_{1,2}$ and $\beta_{1,2}$, then the likelihood function of $LS_{i,1}, \dots, LS_{i,k}$, given $\theta_{1,2}$ and $\beta_{1,2}$, is:

[†] In the Appendix can be found the probability charts of those distributions.

[‡] i is used to denote the belongings of LS to the first ($i = 1$) or second model ($i = 2$) in Eq 2.19.

$$f(LS_{1,1}, \dots, LS_{1,k} | \theta_1, \beta_1) = \left(\frac{1}{\sqrt{2\pi\sigma_{r1}^2}} \right) \exp \left(- \sum_{j=1}^k \left(\frac{LS_{1,j} - \log \theta_1 - \beta_1 n_j}{2\sigma_{r1}^2} \right)^2 \right) \quad 2.22$$

$$S \leq \tilde{s}_{th}$$

$$f(LS_{2,1}, \dots, LS_{2,k} | \theta_2, \beta_2) = \left(\frac{1}{\sqrt{2\pi\sigma_{r2}^2}} \right) \exp \left(- \sum_{j=1}^k \left(\frac{LS_{2,j} - \log \theta_2 - \beta_2 n_j}{2\sigma_{r2}^2} \right)^2 \right) \quad 2.23$$

$$\tilde{s}_{th} \leq S \leq \tilde{a}_{th}$$

Assumed that $\theta_1, \theta_2, \beta_1$ and β_2 are lognormal random variables with parameters defined above, their a posteriori joint distributions, according to the Bayes theorem are:

$$\begin{aligned} f(\theta_1, \beta_1 | LS_{1,1}, \dots, LS_{1,k}) &= \frac{f(LS_{1,1}, \dots, LS_{1,k} | \theta_1, \beta_1) \Pi(\theta_1) \Pi(\beta_1)}{\int_{-\infty}^{+\infty} f(LS_{1,1}, \dots, LS_{1,k} | \theta_1, \beta_1) \Pi(\theta_1) \Pi(\beta_1) d\theta_1 d\beta_1} \\ & \quad S \leq \tilde{s}_{th} \end{aligned} \quad 2.24$$

$$\begin{aligned} f(\theta_2, \beta_2 | LS_{2,1}, \dots, LS_{2,k}) &= \frac{f(LS_{2,1}, \dots, LS_{2,k} | \theta_2, \beta_2) \Pi(\theta_2) \Pi(\beta_2)}{\int_{-\infty}^{+\infty} f(LS_{2,1}, \dots, LS_{2,k} | \theta_2, \beta_2) \Pi(\theta_2) \Pi(\beta_2) d\theta_2 d\beta_2} \\ & \quad \tilde{s}_{th} \leq S \leq \tilde{a}_{th} \end{aligned}$$

Where $f(LS_{1,1}, \dots, LS_{1,k} | \theta_1, \beta_1)$ and $f(LS_{2,1}, \dots, LS_{2,k} | \theta_2, \beta_2)$ are defined in Eq.2.22 and Eq.2.23 respectively and:

$$\begin{aligned} \Pi(\theta_1) &= \left(\frac{1}{\sqrt{2\pi\theta_1^2\sigma_{\theta_1}^2}} \right) \exp \left(- \frac{1}{2} \left(\frac{\log \theta_1 - \mu_{\theta_1}}{\sigma_{\theta_1}} \right)^2 \right) \\ \Pi(\beta_1) &= \left(\frac{1}{\sqrt{2\pi\beta_1^2\sigma_{\beta_1}^2}} \right) \exp \left(- \frac{1}{2} \left(\frac{\log \beta_1 - \mu_{\beta_1}}{\sigma_{\beta_1}} \right)^2 \right) \end{aligned} \quad 2.25$$

$$\Pi(\theta_2) = \left(\frac{1}{\sqrt{2\pi\theta_2^2\sigma_{\theta_2}^2}} \right) \exp \left(- \frac{1}{2} \left(\frac{\log \theta_2 - \mu_{\theta_2}}{\sigma_{\theta_2}} \right)^2 \right)$$

$$\Pi(\beta_2) = \left(\frac{1}{\sqrt{2\pi\beta_2^2\sigma_{\beta_2}^2}} \right) \exp \left(- \frac{1}{2} \left(\frac{\log \beta_2 - \mu_{\beta_2}}{\sigma_{\beta_2}} \right)^2 \right)$$

The a posteriori mean of the parameters can be obtained from:

$$\begin{aligned}\hat{\mu}_{\theta_1} &= \int_{-\infty}^{+\infty} \theta_1 \int_{-\infty}^{+\infty} f(\theta_1, \beta_1 | LS_{1,1}, \dots, LS_{1,k}) d\beta_1 d\theta_1 \\ \hat{\mu}_{\beta_1} &= \int_{-\infty}^{+\infty} \beta_1 \int_{-\infty}^{+\infty} f(\theta_1, \beta_1 | LS_{1,1}, \dots, LS_{1,k}) d\beta_1 d\theta_1 \\ \hat{\mu}_{\theta_2} &= \int_{-\infty}^{+\infty} \theta_2 \int_{-\infty}^{+\infty} f(\theta_2, \beta_2 | LS_{2,1}, \dots, LS_{2,k}) d\beta_2 d\theta_2 \\ \hat{\mu}_{\beta_2} &= \int_{-\infty}^{+\infty} \beta_2 \int_{-\infty}^{+\infty} f(\theta_2, \beta_2 | LS_{2,1}, \dots, LS_{2,k}) d\beta_2 d\theta_2\end{aligned}\quad 2.26$$

And their a posteriori variances from:

$$\begin{aligned}\hat{\sigma}_{\theta_1} &= \int_{-\infty}^{+\infty} (\theta_1 - \hat{\mu}_{\theta_1})^2 \int_{-\infty}^{+\infty} f(\theta_1, \beta_1 | LS_{1,1}, \dots, LS_{1,k}) d\beta_1 d\theta_1 \\ \hat{\sigma}_{\beta_1} &= \int_{-\infty}^{+\infty} (\beta_1 - \hat{\mu}_{\beta_1})^2 \int_{-\infty}^{+\infty} f(\theta_1, \beta_1 | LS_{1,1}, \dots, LS_{1,k}) d\beta_1 d\theta_1 \\ \hat{\sigma}_{\theta_2} &= \int_{-\infty}^{+\infty} (\theta_2 - \hat{\mu}_{\theta_2})^2 \int_{-\infty}^{+\infty} f(\theta_2, \beta_2 | LS_{2,1}, \dots, LS_{2,k}) d\beta_2 d\theta_2 \\ \hat{\sigma}_{\beta_2} &= \int_{-\infty}^{+\infty} (\beta_2 - \hat{\mu}_{\beta_2})^2 \int_{-\infty}^{+\infty} f(\theta_2, \beta_2 | LS_{2,1}, \dots, LS_{2,k}) d\beta_2 d\theta_2\end{aligned}\quad 2.27$$

Since the solution to the problem stated has not been found in the statistical literature and recognizing the computation problem associated with solving the equations numerically, we have to make other assumptions on the parameters' pdf functional forms. In order to reduce problem complexity the assumption of β_1 and β_2 as normal distributed parameters is reasonable. This assumption let us to exploit the problem solution proposed by Lindley (D. V. Lindley, 1972) and Gebraeel (N. Gebraeel J. P., 2008). Therefore, $\log \theta_1, \log \theta_2, \beta_1$ and β_2 are assumed to be normal random variables with parameters:

$$\begin{aligned}\log \theta_1 = \omega_1 &= N(\mu_{\omega_1}, \sigma_{\omega_1}) & \log \theta_2 = \omega_2 &= N(\mu_{\omega_2}, \sigma_{\omega_2}) \\ \beta_1 &= N(\mu_{\beta_1}, \sigma_{\beta_1}) & \beta_2 &= N(\mu_{\beta_2}, \sigma_{\beta_2})\end{aligned}$$

Before proceeding to the formal definition of the problem statement, an assessment of the errors computed after relaxing the hypothesis of lognormal distributed β_1 and β_2 can be done through a comparison of the a priori TTF calculated by the model with β_1 and β_2 as normal random variables with the true TTF computed through the crack growth simulations.

The a priori TTF probability distribution, given the model described by the Eq.2.20, can be computed as the probability that the degradation signal (crack size) LS is smaller than the crack maximum size allowed for each cycle $n_i > 0$, given the a priori model parameters pdfs. The statement, remembering the Eq.2.18, can be formally written as,

$$TTF(n_k = 0) = \hat{T}_1 + \hat{T}_2 \quad 2.28$$

Where \hat{T}_1 and \hat{T}_2 are the a priori pdf distributions of T_1 and T_2 . They can be expressed as:

$$\begin{aligned}\hat{T}_1(n_i | n_k = 0) \\ = P(LS_1(n_i) \geq \tilde{S}_{th} | \hat{\omega}_1, \hat{\beta}_1)\end{aligned}\quad 2.29$$

$$\begin{aligned}\hat{T}_2(n_j | n_k = 0) \\ = P(LS_2(n_j) \geq \tilde{a}_{th} | \hat{\omega}_2, \hat{\beta}_2)\end{aligned}\quad 2.30$$

Where $\hat{\omega}_1, \hat{\beta}_1, \hat{\omega}_2$ and $\hat{\beta}_2$ are the a priori pdf of $\omega_1, \omega_2, \beta_1$ and β_2 respectively.

Given that $\hat{\omega}_1, \hat{\omega}_2, \hat{\beta}_1$ and $\hat{\beta}_2$ are normal random variables, the degradation signal LS_1 and LS_2 computed at cycles n_i and n_j respectively, are normal variables as well (N. Gebraeel J. P., 2008)(N. Gebraeel M. L., 2005)(C.J. Lu, 1993) with mean variance given by:

$$\begin{aligned}\mu_{LS_1}(n_i) &= \mu_{\omega_1} + \mu_{\beta_1} n_i \\ \sigma_{LS_1}^2(n_i) &= \sigma_{\omega_1}^2 + \sigma_{\beta_1}^2 n_i^2 \\ &\quad + 2\rho_1 \sigma_{\omega_1} \sigma_{\beta_1} + \sigma_{r_1}^2\end{aligned}\quad 2.31$$

$$\begin{aligned}\mu_{LS_2}(n_j) &= \mu_{\omega_2} + \mu_{\beta_2} n_j \\ \sigma_{LS_2}^2(n_j) &= \sigma_{\omega_2}^2 + \sigma_{\beta_2}^2 n_j^2 \\ &\quad + 2\rho_2 \sigma_{\omega_2} \sigma_{\beta_2} + \sigma_{r_2}^2\end{aligned}\quad 2.32$$

Remembering the Eq.2.29 and 2.30, we can write for \hat{T}_1 :

$$\begin{aligned}\hat{T}_1(n_i | n_k = 0) &= \\ &= 1 - P(LS_1(n_i) \leq \tilde{S}_{th} | \hat{\omega}_1, \hat{\beta}_1) = \\ &= 1 - P\left(Z < \frac{\tilde{S}_{th} - \mu_{LS_1}(n_i)}{\sqrt{\sigma_{LS_1}^2(n_i)}}\right) \\ &= \Phi\left(\frac{\tilde{S}_{th} - \mu_{LS_1}(n_i)}{\sqrt{\sigma_{LS_1}^2(n_i)}}\right)\end{aligned}\quad 2.33$$

And for \hat{T}_2 :

$$\begin{aligned}
 \hat{T}_2(n_j | n_k = 0) &= \\
 1 - P(\text{LS}_2(n_j) \leq \tilde{a}_{th} | \hat{\omega}_1, \hat{\beta}_1) &= \\
 = 1 - P\left(Z < \frac{\tilde{a}_{th} - \mu_{\text{LS}_1}(n_i)}{\sqrt{\sigma^2_{\text{LS}_1}(n_i)}}\right) & \\
 = \Phi\left(\frac{\tilde{a}_{th} - \mu_{\text{LS}_2}(n_j)}{\sqrt{\sigma^2_{\text{LS}_2}(n_j)}}\right) & \quad 2.34
 \end{aligned}$$

Where Φ stands for the standard normal cdf. The domain of \hat{T}_1 and \hat{T}_2 , is ≤ 0 , thus can take on negative values, which is practically impossible from an implementation standpoint. Consequently, we use the truncated cdf for \hat{T}_1 and \hat{T}_2 with the constraint $\hat{T}_i \geq 0$, $i=1,2$ which is given as:

$$\begin{aligned}
 \hat{T}_1 &= \frac{\hat{T}_1 - \hat{T}_1(n_i = 0)}{\hat{T}_1(n_i = 0)} \\
 \hat{T}_2 &= \frac{\hat{T}_2 - \hat{T}_2(n_j = 0)}{\hat{T}_2(n_j = 0)} \quad 2.35
 \end{aligned}$$

As observed by (N. Gebraeel M. L., 2005), \hat{T}_1 and \hat{T}_2 are three parameter truncated Bernstein distributed random variables for which the first and second moment closed form don't exist (A.K. Sheikh, 1983). As suggested by (N. Gebraeel M. L., 2005) the median is taken as the central moment. This can be justified, from one side by the not-existence of a closed form for the mean, and for the other hand, considering that the T_i pdfs are skewed and therefore the use of the median is more appropriate and conservative.

To compute the sum of the two random variables the Monte Carlo technique is followed, given the \hat{T}_1 and \hat{T}_2 numerical pdfs shown in Figure 15. The $\hat{\omega}_1, \hat{\beta}_1, \hat{\omega}_2$ and $\hat{\beta}_2$ a priori pdfs parameters are reported in Table 4.

	$\hat{\omega}_1$	$\hat{\beta}_1$	$\hat{\omega}_2$	$\hat{\beta}_2$	ϵ_1	ϵ_2
μ	-10.35	6.95e-009	-8.85	1.07e-007	0	0
σ^2	0.69	6.92e-035	47.65	3.55e-029	1.76e-008	1.5e-005
ρ	-0.1421		-0.2039			

Table 4 $\hat{\omega}_1, \hat{\beta}_1, \hat{\omega}_2$ and $\hat{\beta}_2$ a priori pdfs parameters

The pdfs are simply obtained differentiating the two cdfs with respect to n .

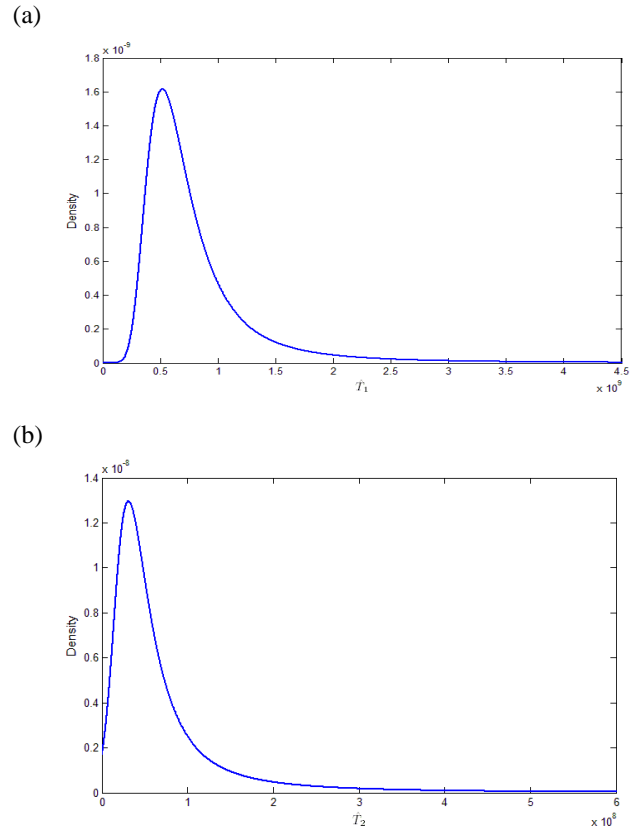


Figure 15 (a) \hat{T}_1 pdf (b) \hat{T}_2 pdf

Eventually the modeled a priori TTF is shown in Figure 16 compared to the simulated a priori TTF on a lognormal probability plot. The green circles belong to the simulated a priori TTF, while the black ones belong to the modeled a priori TTF.

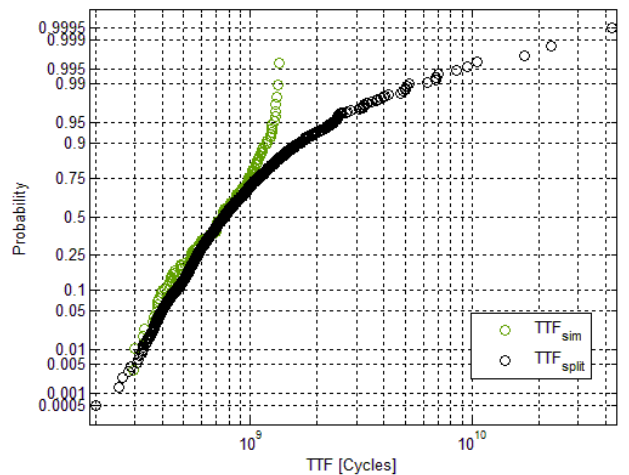


Figure 16 Simulated a priori TTF and a priori modeled TTF comparison – probability plot

A further comparison is between the two TTF pdfs is shown in Figure 17 in which both the cdfs are plotted. From the two figures can be observed that the left hand distributions' tail are similar, while for large values of TTF the two distributions differs. The modeled TTF has the right hand tail longer than the simulated one. However, for our purposes the left hand tail is much more important than the right one. For this reason the $\hat{\beta}_1$ and $\hat{\beta}_2$ normality assumption can be acceptable.

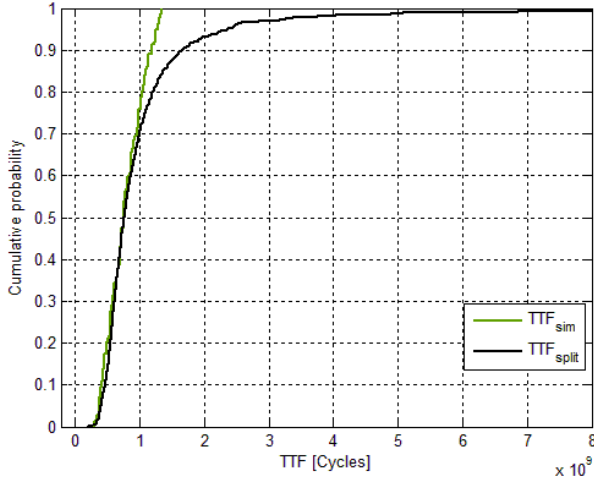


Figure 17 Simulated a priori TTF and a priori modeled TTF comparison – cdf

It is worth noting that if the two model's parameters are somehow correlated, It would be possible to update the second model's parameter instead of using the a priori information to compute the TTF till the threshold \hat{S}_{th} is reached. This situation would be valuable to exploit because better predictions could be performed since the beginning of the crack growth. Unfortunately this is not the case since the two pairs of coefficients are not significantly correlated as can be observed from Figure 18.

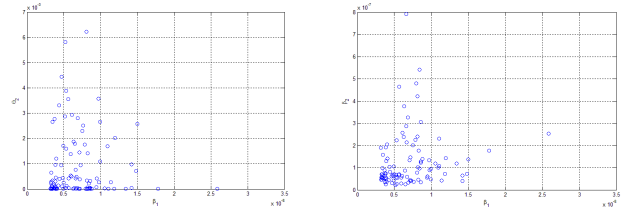
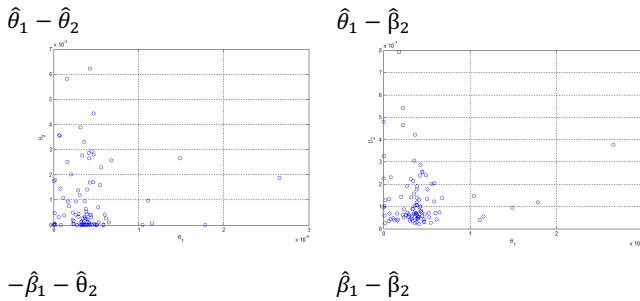


Figure 18 Correlations between the couple of model parameters

Now, once we have computed the a priori parameters' pdfs, we can write the equations that update these pdfs' parameters once obtained the signals $LS_{1,1}, \dots, LS_{1,k}$ or $LS_{2,1}, \dots, LS_{2,k}$ from the monitoring system, depending in which S interval the signals are. Below is just reported the final formulas from which the updated pdfs parameters are obtained.

The models can be rewritten as:

$$\begin{cases} LS_1 = X_1[A]_1 \\ LS_2 = X_2[A]_2 \end{cases} \quad \begin{matrix} S \leq \tilde{S}_{th} \\ \tilde{S}_{th} \leq S \leq \\ \tilde{a}_{th} \end{matrix} \quad 2.36$$

Where:

$$\begin{aligned} [A]_1 &= \begin{bmatrix} \omega_1 \\ \beta_1 \end{bmatrix} & X_1 &= \begin{bmatrix} 1 & n_1 \\ \vdots & \vdots \\ 1 & n_n \end{bmatrix} & [A]_2 &= \begin{bmatrix} \omega_2 \\ \beta_2 \end{bmatrix} & X_2 &= \begin{bmatrix} 1 & n_{1,2} \\ \vdots & \vdots \\ 1 & n_{n,2} \end{bmatrix} \end{aligned}$$

At a cycle n_t , given the measures $LS_{i,1}, LS_{i,2}, \dots, LS_{i,t}$, $i = 1,2$ the updated $\omega_1, \beta_1, \omega_2, \beta_2$ pdfs parameters are:

$$\begin{aligned} \tilde{\mu}_1^T &= \left(\left[(X_1^T X_1)^{-1} X_1^T LS_1 \right]^T \frac{X_1^T X_1}{\sigma_{r1}^2} \right. \\ &\quad \left. + \hat{\mu}_1^T \hat{\Sigma}_1^{-1} \right) \left(\frac{X_1^T X_1}{\sigma_{r1}^2} \right. \\ &\quad \left. + \hat{\Sigma}_1^{-1} \right)^{-1} \end{aligned} \quad 2.37$$

$$\hat{\Sigma}_1 = \left(\frac{X_1^T X_1}{\sigma_{r1}^2} + \hat{\Sigma}_1^{-1} \right)^{-1} \quad 2.38$$

$$\begin{aligned} \tilde{\mu}_2^T &= \left(\left[(X_2^T X_2)^{-1} X_2^T LS_2 \right]^T \frac{X_2^T X_2}{\sigma_{r2}^2} \right. \\ &\quad \left. + \hat{\mu}_2^T \hat{\Sigma}_2^{-1} \right) \left(\frac{X_2^T X_2}{\sigma_{r2}^2} \right. \\ &\quad \left. + \hat{\Sigma}_2^{-1} \right)^{-1} \end{aligned} \quad 2.39$$

$$\tilde{\Sigma}_2 = \left(\frac{X_2^T X_2}{\sigma_{r2}^2} + \hat{\Sigma}_2^{-1} \right)^{-1} \quad 2.40$$

Where:

$$\begin{aligned} \hat{\mu}_1 &= [\mu_{\omega 1} \quad \mu_{\beta 1}] & \hat{\mu}_2 &= [\mu_{\omega 2} \quad \mu_{\beta 2}] \\ \hat{\Sigma}_1 &= \begin{bmatrix} \sigma_{\omega 1} & \sigma_{\omega 1, \beta 1} \\ \sigma_{\omega 1, \beta 1} & \sigma_{\beta 1} \end{bmatrix} & \hat{\Sigma}_2 &= \begin{bmatrix} \sigma_{\omega 2} & \sigma_{\omega 2, \beta 2} \\ \sigma_{\omega 2, \beta 2} & \sigma_{\beta 2} \end{bmatrix} \end{aligned}$$

are the vectors of the a priori pdfs means and the covariance matrixes while:

$$\begin{aligned} \tilde{\mu}_1 &= [\tilde{\mu}_{\omega 1} \quad \tilde{\mu}_{\beta 1}] & \tilde{\mu}_2 &= [\tilde{\mu}_{\omega 2} \quad \tilde{\mu}_{\beta 2}] \\ \tilde{\Sigma}_1 &= \begin{bmatrix} \tilde{\sigma}_{\omega 1} & \tilde{\sigma}_{\omega 1, \beta 1} \\ \tilde{\sigma}_{\omega 1, \beta 1} & \tilde{\sigma}_{\beta 1} \end{bmatrix} & \tilde{\Sigma}_2 &= \begin{bmatrix} \tilde{\sigma}_{\omega 2} & \tilde{\sigma}_{\omega 2, \beta 2} \\ \tilde{\sigma}_{\omega 2, \beta 2} & \tilde{\sigma}_{\beta 2} \end{bmatrix} \end{aligned}$$

are the vectors of the a posteriori pdfs means and the covariance matrixes.

Now, given the a posteriori pdfs' parameters the T_1 or T_2 distribution can be computed.

Remembering Eq.2.31 and 2.32 the updated mean and the variance of the degradation signal at a cycle n_i or n_j will be:

$$\tilde{\mu}_{LS_1}(n_i) = \tilde{\mu}_{\omega 1} + \tilde{\mu}_{\beta 1} n_i \quad 2.41$$

$$\tilde{\sigma}_{LS_1}^2(n_i) = \tilde{\sigma}_{\omega 1}^2 + \tilde{\sigma}_{\beta 1}^2 n_i^2 + 2\tilde{\rho}_{\omega 1} \sigma_{\omega 1} \tilde{\sigma}_{\beta 1} + \sigma_{r1}^2$$

$$\tilde{\mu}_{LS_2}(n_j) = \tilde{\mu}_{\omega 2} + \tilde{\mu}_{\beta 2} n_j \quad 2.42$$

$$\tilde{\sigma}_{LS_2}^2(n_j) = \tilde{\sigma}_{\omega 2}^2 + \tilde{\sigma}_{\beta 2}^2 n_j^2 + 2\tilde{\rho}_{\omega 2} \tilde{\sigma}_{\omega 2} \tilde{\sigma}_{\beta 2} + \sigma_{r2}^2$$

And therefore from Eq.2.33 and 2.34 the updated T_1 or T_2 pdf will be:

$$\begin{aligned} \tilde{T}_1(n_i | LS_{1,1} \quad LS_{1,2}, \dots, LS_{1,t}) \\ = \Phi \left(\frac{\tilde{S}_{th} - \mu_{LS_1}(n_i)}{\sqrt{\sigma_{LS_1}^2(n_i)}} \right) \quad 2.43 \\ \xrightarrow{\tilde{r}_1 \geq 0} \frac{\tilde{T}_1 - \tilde{T}_1(0)}{\tilde{T}_1(0)} \end{aligned}$$

And for \tilde{T}_2 :

$$\begin{aligned} \tilde{T}_2(n_j | LS_{2,1} \quad LS_{2,2}, \dots, LS_{2,t}) \\ = \Phi \left(\frac{\tilde{a}_{th} - \mu_{LS_2}(n_j)}{\sqrt{\sigma_{LS_2}^2(n_j)}} \right) \quad 2.44 \\ \xrightarrow{\tilde{r}_2 \geq 0} \frac{\tilde{T}_2 - \tilde{T}_2(0)}{\tilde{T}_2(0)} \end{aligned}$$

An Example:

Given a crack growth path shown in Figure 19, at each time step we can update the a priori TTF given in Figure 2, exploiting the information gained from monitoring the crack growth.

Using Eq.2.37, 2.38 for the first part of the degradation pattern (T_1 in Figure 19) and the Eq.2.39 and 2.40 for the second part, we can compute the a posteriori $\hat{\omega}_1, \hat{\beta}_1, \hat{\omega}_2$ and $\hat{\beta}_2$ pdfs' parameters, that are the means and the standard deviations.

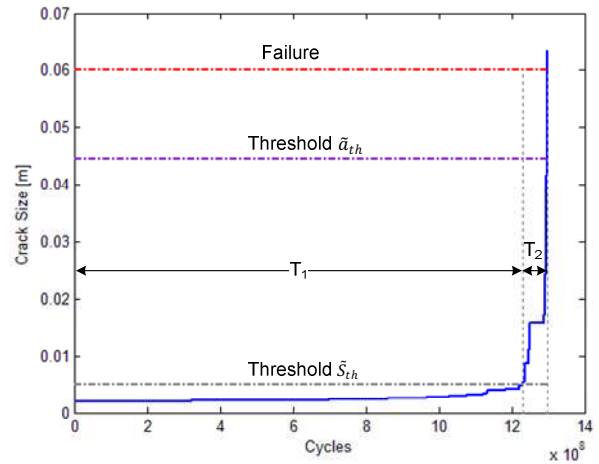
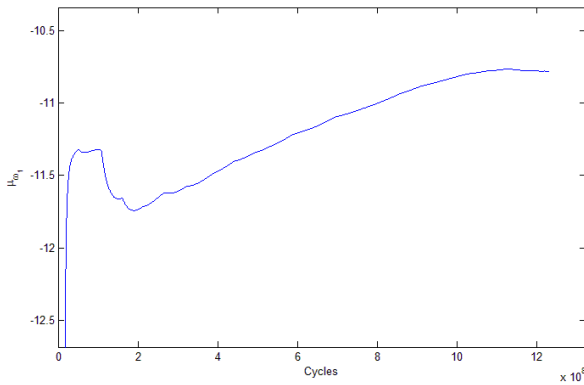


Figure 19 Crack growth path

From the initial cycle to that one that corresponds to a crack size of 5.1 mm the updated TTF is given by Eq.2.7 where T_2 is given by Eq.2.35, that is the a priori modeled T_2 .

a)



b)

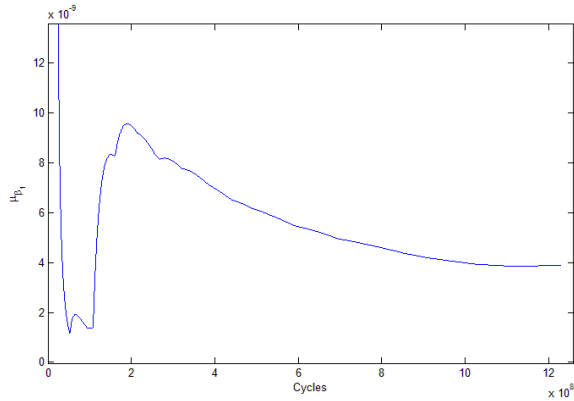


Figure 20 a) updated $\tilde{\mu}_{\omega 1}$ and b) updated $\tilde{\mu}_{\beta 1}$

b) shows the updated $\tilde{\mu}_{\omega 1}$ as a function of cycles, while the plot b) shows the updated $\tilde{\mu}_{\beta 1}$.

At each time step, given the updated $\tilde{\mu}_{\omega 1}$ and $\tilde{\mu}_{\beta 1}$ we can compute the a actual TTF where \tilde{T}_1 is given by the Eq.2.43. For each time step the TTF median and the 1st percentile is stored. These two values are plotted in Figure 21. As can be observed, cycle after cycle the predictions converge to the true TTF even before the second degradation phase. In this case, both the 1st percentile and the mean fall within the 5% error interval. The interval in which the TTF median and its 1st percentile lines are interrupted means that the predicted TTF falls beyond the timescale.

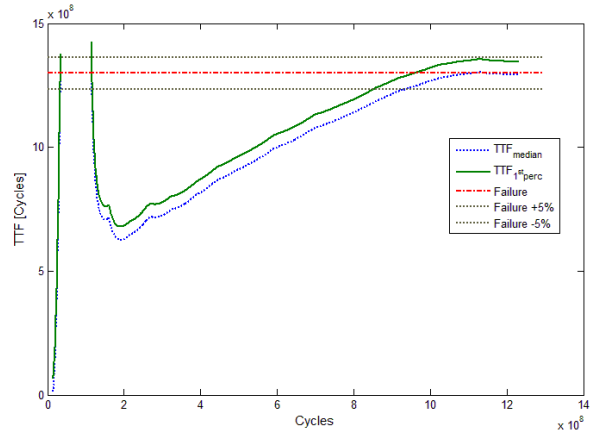


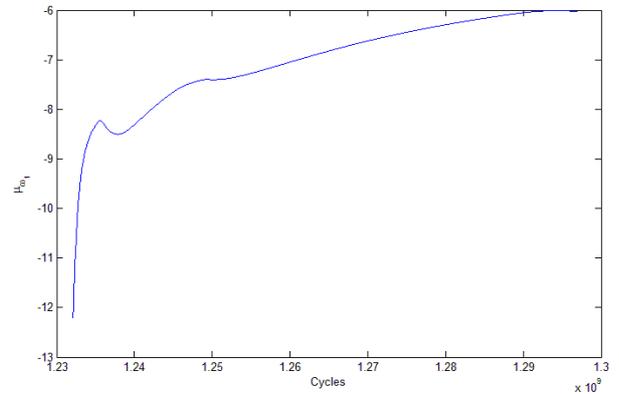
Figure 21 Predicted TTF - 1st phase

Once the threshold \tilde{S}_{th} is passed, the TTF is equal to the cycle T_1 , that is no more a random variable (it is deterministic), plus the predicted \tilde{T}_2 .

\tilde{T}_2 is given by Eq.2.44, once computed the updated $\mu_{\beta 2}$, $\mu_{\omega 2}$ and the related variances given by Eq.2.39 and 2.40.

Figure 22 shows the updated $\mu_{\beta 2}$ and $\mu_{\omega 2}$ respectively.

a)



b)

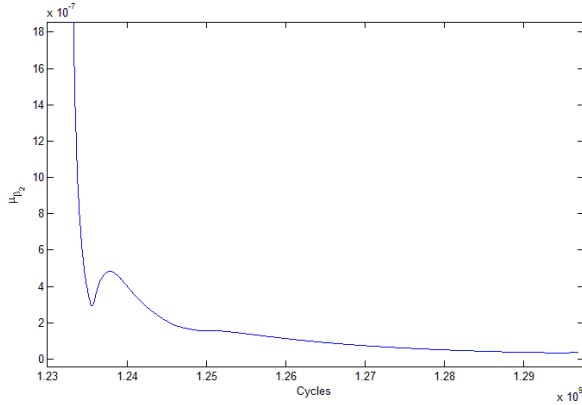


Figure 22 a) updated $\tilde{\mu}_{\omega 2}$ and b) updated $\tilde{\mu}_{\beta 2}$

As previously done for the first degradation phase, the *TTF* pdf can be computed using Eq.2.39, 2.40, 2.42 and eventually 2.44. The updated *TTF* median and its 1st percentile are shown in Figure 23.

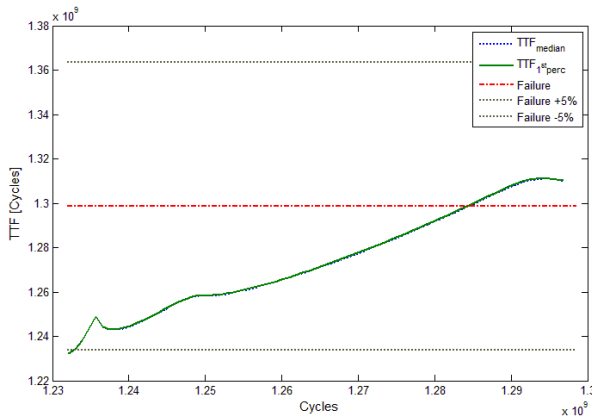


Figure 23 Predicted *TTF* – 2nd phase

Can be observed how the predictions converge to actual failure time. This time the prediction variances are smaller than those of the first phase. This is due to the fact that the 1st phase predictions include the uncertainties related to the a priori T_2 pdf.

2.3.3 Prognostic through the physical model

The same problem faced by the Bayesian prognostic model can be pursued through a recursive application of the crack growth model presented in paragraph 2.1. The physical phenomenon analyzed in this context has been faced by numerous researches, therefore numerous models have been proposed capable of describing and highlighting the main variables and their relations that influence the crack growth. The NASGRO model used in this context is recognized to be the most reliable to describe crack growth in railway

axles(S. Beretta M. C., 2006)(U. Zerbst M. V., 2005)(S. Beretta M. C., 2004), therefore can be used to predict accurately the *TTF*.

The main idea at the basis of this approach is that, once measured and estimated the actual crack size and the loads history, we can estimate the *TTF* through simulating the possible growth paths by using a Monte Carlo technique.

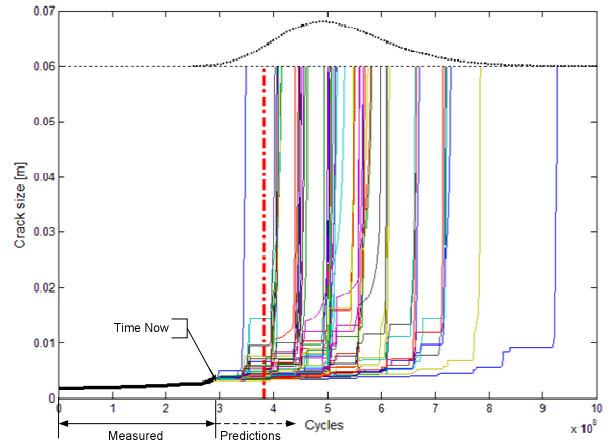


Figure 24 *TTF* prediction through the NASGRO crack growth model

This approach is shown in Figure 24. Let suppose that through the monitoring infrastructure we have measured the crack size at the time now, we can simulate the crack propagation considering as random variables the load applied and the SIF threshold and the initial crack size equal to the measured one. The functions plotted and originating from the time now, are some simulated crack growth paths. Starting from the crack growth paths set, it is possible to estimate the *TTF* pdf. In Figure 24 the black dotted line represents the predicted *TTF* pdf, while the red line represents the actual failure time.

The estimated *TTF* at each time step can be approximated by lognormal distribution, as shown in Figure 25.

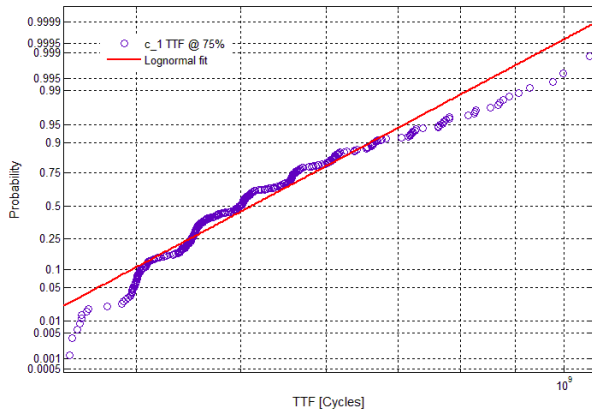


Figure 25 The approximated TTF probability plot

As in the Bayesian approach, at each time step, the *TTF* 1st percentile, the median and the *TTF* at 98% level of confidence is stored. However, for computational reasons, the *TTF* updating times are set at the 5%, to the 99% of the actual *TTF* with a 5% gap. Figure 27 shows the *TTF* estimations at different time steps. Can be observed how the predictions converge to the actual failure. At the last updating time step all the *TTF* distributions's lower and upper bounds fall into the 5% error interval.

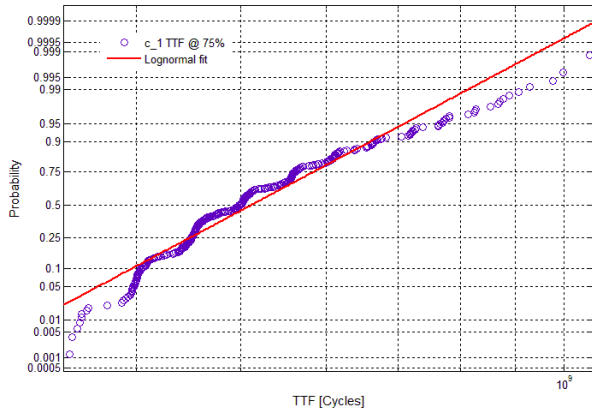


Figure 26 The approximated TTF probability plot

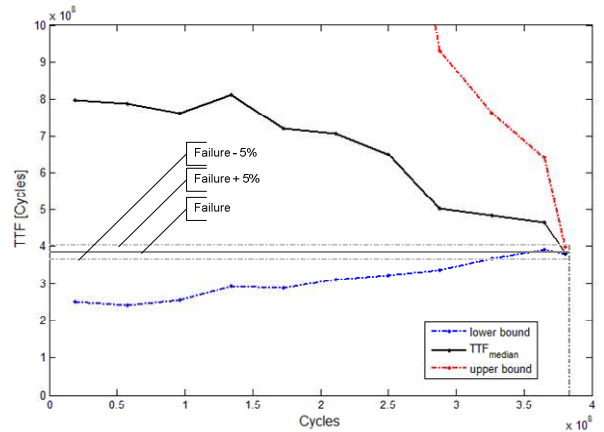


Figure 27 TTF predictions

Figure 28 shows how the confidence interval diminish as we approach to the actual failure. The green dotted line represents the difference between the *TTF* median and the *TTF* at the 0.01 confidence level, while the red dashed dotted line represents the *TTF* pdf upper bound, at the 0.99 confidence level.

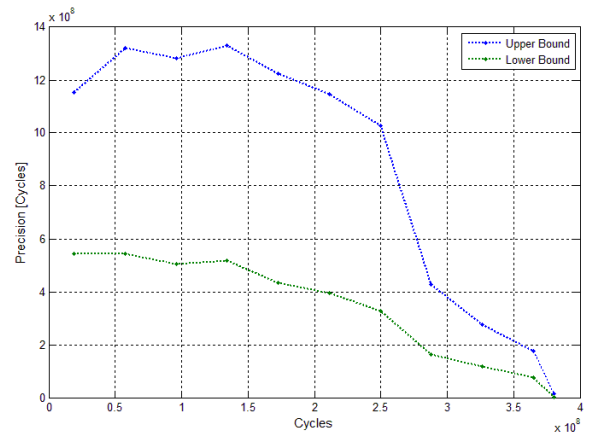


Figure 28 Estimated TTF at the 0.01 and 0.98 confidence level

2.3.4 The size error and the updating frequency effect on TTF predictions

In the case of the physical model, the size error and the updating frequency effect on the estimations can be approximately evaluated through simple geometrical considerations. The assessment of these effects on the predictions performances is an important issue since they characterize the monitoring and diagnostic equipment goodness. Higher size errors characterize low performance diagnostic, while lower updating frequency entails lower monitoring equipment cost.

In this case the effect of the updating frequency on the prediction performances is not relevant since the TTF estimation relies on just the last crack size measurement and not, as in the Bayesian case, on the complete set of measurements. The TTF updating frequency effect can be considerable when maintenance scheduling decisions is considered. By this point of view, high frequency updating is preferable since the decisions can be based on an updated TTF .

In this case we can apply a predictive maintenance policy similar to that one proposed by Kaiser et.al. in (N.Z Gebraeel, 2009). The stopping rule, i.e the cycle n_k at which the axle should be substituted, is defined as in Eq.2.45.

$$n_k \rightarrow TTF_{lb}(n_k) - n_k - \delta \leq 0 \quad 2.45$$

Where n_k is the first cycle at which the rule is verified, $TTF_{lb}(n_k)$ is the TTF prediction computed at a 0.01 confidence level at the cycle n_k , δ is the updating interval. From this simple rule is self-evident that the greater δ the lower n_k .

This simple rule can be easily understood by analyzing the graph shown in Figure 29. The blue line represents the estimated TTF at the 0.01 confidence level while the black dotted line represents the equality $n = TTF_{lb}$. The dashed line represents the equality $n = TTF_{lb} + \delta$. Therefore, for Eq.2.45, the cycle n_k is the first intersection point of the TTF_{lb} (blue line) with the black dashed line. Particularly, referring to what stated in the previous chapters, the quantity $TTF_{lb}(n_k) - n_k$ is the RUL computed at the 0.01 confidence level (RUL₋ in Figure 29). The main idea associated with this rule is that the axle can be safely run till it reaches the last TTF_{lb} estimation.

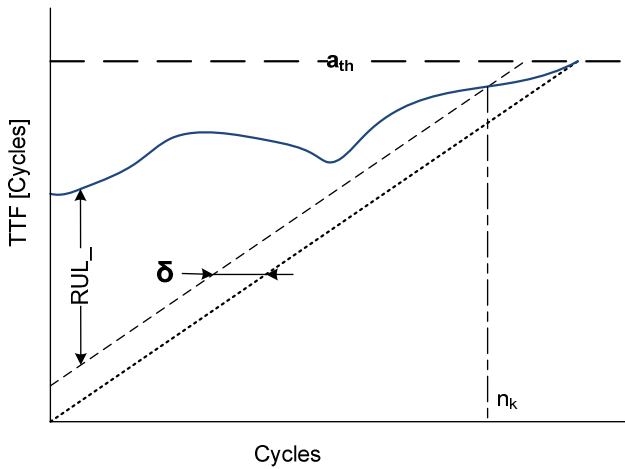


Figure 29 The effect of updating frequency on TTF predictions

The size error effect on the TTF predictions can be approximately computed making the hypothesis that the crack growth path can be approximated with an exponential function. Generally, as described in 2.3.1, the more the size error the lesser the threshold. The analysis framework is shown in Figure 30. Let us suppose that for a given size error, the failure threshold is set at the value a_{th} and that we are at the cycle n_i and we measure the crack size $\exp(LS_i)$. Through the method explained in paragraph 2.3.3, we can compute the TTF pdf (blue line) and therefore we know the TTF_{median} and the TTF_{1stp} at the 0.01 confidence level.

Next, suppose that the new size error is greater to the previous one, consequently, from Eq.2.17 keeping a_{max} constant, we obtain the failure threshold a_{th2} lower than a_{th} . This threshold shift causes a change in the TTF pdf parameters and therefore to the reference points TTF_{median} and TTF_{1stp} .

The new reference points TTF'_{median} and TTF'_{1stp} computed at cycle n_i , thanks to the hypothesis made, can be computed as follows:

$$TTF'_{median} = TTF_{median} - \frac{\log a_{th} - \log a_{th2}}{\beta} \quad 2.46$$

$$TTF'_{1stp} = TTF_{1stp} - \frac{\log a_{th} - \log a_{th2}}{\alpha} \quad 2.47$$

Where:

$$\alpha = \frac{\log a_{th} - LS_i}{TTF_{1stp} - n_i} \quad 2.48$$

$$\beta = \frac{\log a_{th} - LS_i}{TTF_{1stp} - n_i} \quad 2.49$$

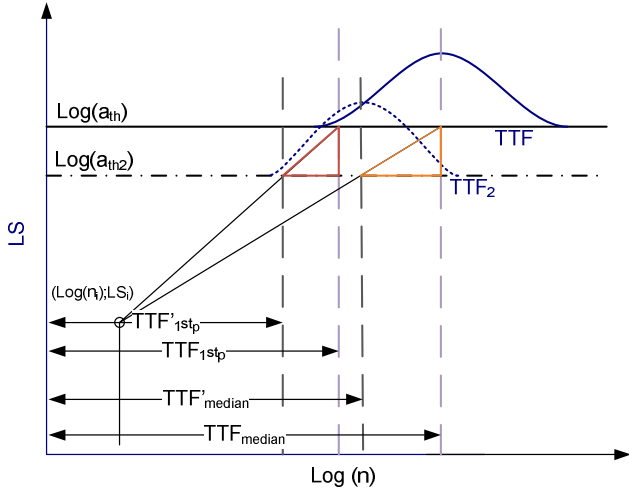


Figure 30 The error size effect on TTF predictions

The lower confidence interval $CI = (TTF_{median} - TTF_{1stp})$, decreases when the size error increases, i.e the prediction is more accurate. This can be easily demonstrated, subtracting term by term Eq. 2.46 with Eq. 2.47 we obtain:

$$CI' = CI - \Delta(\log a_{th}) \left(\frac{1}{\beta} - \frac{1}{\alpha} \right) \quad 2.50$$

Since $\beta < \alpha$ and $\Delta(\log a_{th}) > 0$ for increasing size errors $CI' < CI$.

It is worth noting that, from Eq. 2.47, the ratio $\frac{TTF_{1stp}}{TTF'_{1stp}}$ is not linear with respect to the ratio $\frac{a_{th}}{a_{th2}}$ and from Eq.2.17 the ratio $\frac{a_{th}}{a_{th2}}$ is not a linear function of the size error ratio.

The updating frequency and size error combined effect on the cycle n_k normalized with respect the actual failure (i.e % of the life exploited) on particular crack growth curve is shown in Figure 31. As we can see the relationship between the size error and the ratio $\frac{n_k}{n_{failure}}$. As the size error increases, for a given updating frequency, the life exploited decreases, while the relationship between the updating frequency and the life exploited for a given size error is linear: the more frequent the TTF updating the greater the life exploited.

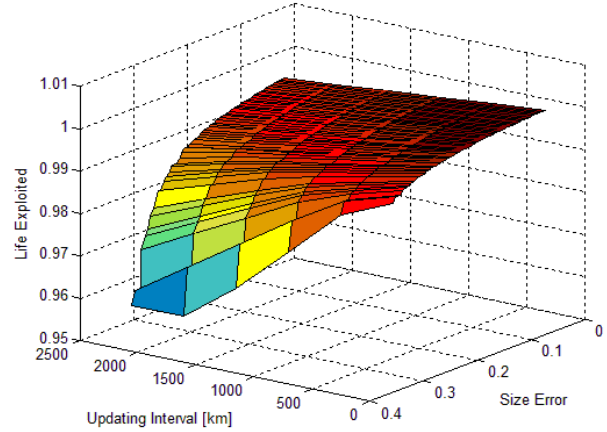


Figure 31 The updating frequency and size error combined effect

3. RESULTS

Our goal, as stated in paragraph 2, is to assess the predictive performances of both the prognostic models and eventually highlight the differences between the predictive and preventive maintenance policy.

The probabilistic aspect of the issue has clearly arisen during the dissertation, therefore a reliable and a definitive answer to the questions proposed has to be given after numerous simulations that guarantee a reliable representation of the probabilistic aspects involved. However, some preliminary considerations can be outlined analyzing a limited number of instances.

The method used to select the instances analyzed is based on the stratified sampling technique. Particularly, the TTF pdf represented in Figure 2 has been divided in 10 equal spaced intervals, that corresponds to the bins shown in the same figure. For each bin a crack growth path was selected obtaining a set of 10 possible degradation curves as shown in Figure 32.

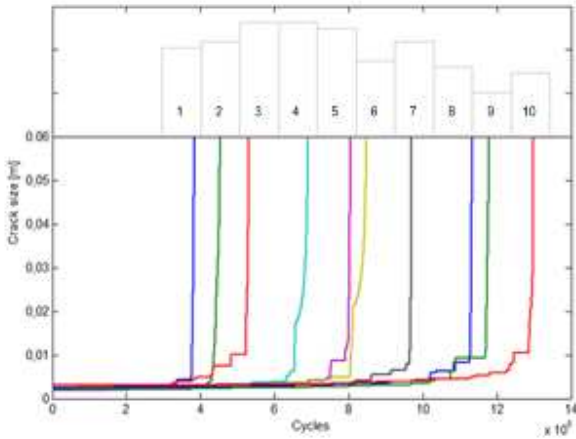


Figure 32: The 10 crack growth paths

For the whole set of track selected, the Bayesian prognostic algorithm and the physical model was applied. Moreover, the maximum number of inspections N_{insp} and the expected number of inspections \bar{N}_{insp} was computed.

In order to evaluate the prognostic algorithms described, two metrics were used, one of which suggested by (A.Saxena, 2008).

This metric, called Timeliness φ , exponentially weighs RUL prediction errors through an asymmetric weighting function. Penalizes the late predictions more than early prediction. The formula is:

$$\Phi(n) = \begin{cases} \exp\left(\frac{|z(n)|}{a}\right) & z \geq 0 \\ \exp\left(\frac{|z(n)|}{b}\right) & z \leq 0 \end{cases} \quad 3.1$$

$$\varphi = \frac{1}{N} \sum_{n=1}^N \Phi(n) \quad 3.2$$

Where $z(n) = TTF_{actual} - TTF_{median}(n)$ is the prediction error computed at cycle n , while a and b are two constants where $a > b$. In this case $a = 100$ and $b = 10$.

Ideally the perfect score is $\varphi=1$. To be comparable, the updating frequency has to be the same between the two algorithms, therefore the TTF predictions in the physical model case have been linearly interpolated.

The other metric chosen is simply the predictions percentage error computed at fixed time steps $n_k = 0.25FT, 0.5FT, 0.75FT, 0.98FT$, where FT is the cycle at which the failure occurs.

In the appendix the comparison of the predictions at different time steps and the PC_{DET} for each of 10 sampled

paths can be found. Moreover, the size error and the updating frequency effect on the exploited life are plotted for each instance.

As can be noticed from these figures, both the algorithms' predictions converge to the actual failure time. The information about the actual degradation path increase as time elapses, resulting in an improved knowledge about the actual TTF. Better knowledge of the crack growth behavior allow more accurate predictions. The advantage of continuous monitoring with respect to the a priori information is clearly evident observing Figure 33. It shows the TTF pdf obtained from the prognostic algorithms described and the a priori TTF pdf (black line). It is clearly noticeable how prognostics can improve the knowledge on the actual failure path followed by an individual axle.

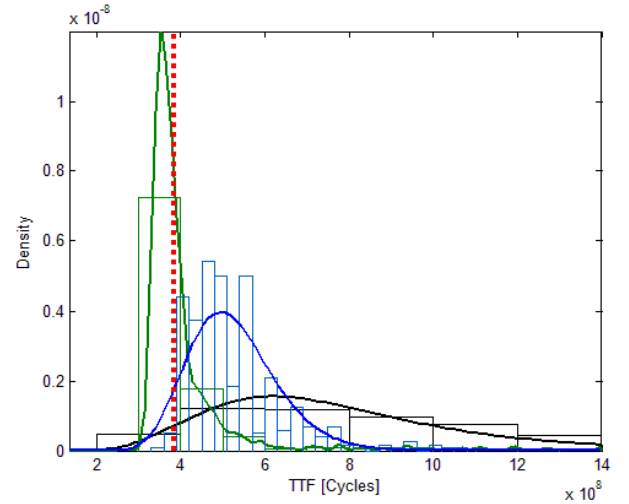


Figure 33 Comparison of the a priori TTF pdf and the updated TTF pdf obtained from the prognostics algorithms described (green-Bayesian, blue physical based model, black - a priori)

However, substantial differences among the two prognostic approach exists. Particularly, what differs is the distribution of the prediction errors along the degradation timeline and the prediction confidence interval. The last statement is evident observing the figures in the appendix in which the predictions paths are compared. In all the instances selected the physical model confidence interval is larger than that one computed by the Bayesian approach.

However, the most important differences among the two approaches have to be evaluated in term of the prediction errors. The following graphs display the prediction errors for both the algorithms and for the whole crack growth track set at fixed residual life percentile (i.e 0.25, 0.5, 0.75, 0.98). The same information are displayed in a tabular form in Table 5. The percentage prediction error is simply calculated as:

$$err\% = \frac{FT - TTF_{median}}{FT} 100 \quad 3.3$$

From the graphs can be concluded that:

1. Physical model prediction errors decrease approaching the FT
2. Bayesian algorithm prediction errors decreases till the 75^o percentile of the residual lifetime, while at 98% the errors are greater that in the 75 percentile
3. Physical model predictions are lower for FT near the average (bins 3,4,5)
4. Bayesian predictions seems to outperform the physical model predictions for till the 75th percentile, while for the 98th the physical model predictions are more accurate.

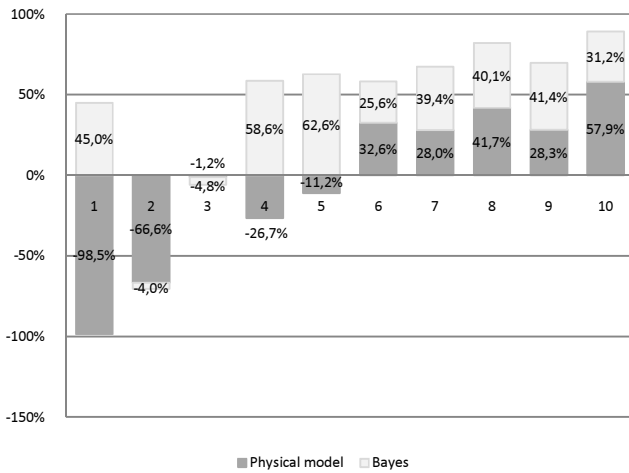


Figure 34 Percentage prediction error @ 25% FT

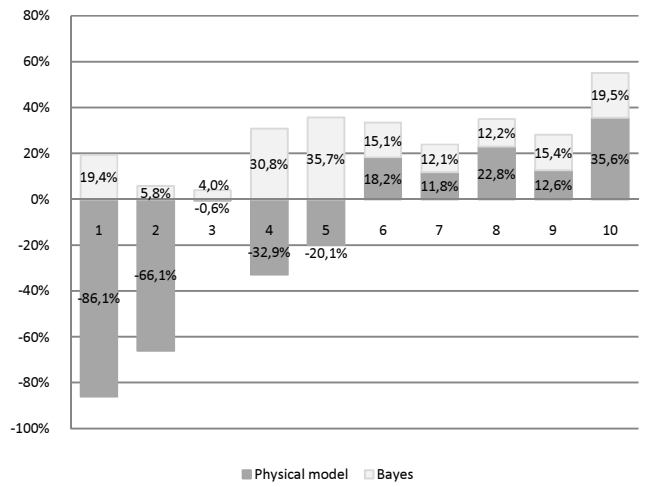


Figure 35 Percentage prediction error @ 50% FT

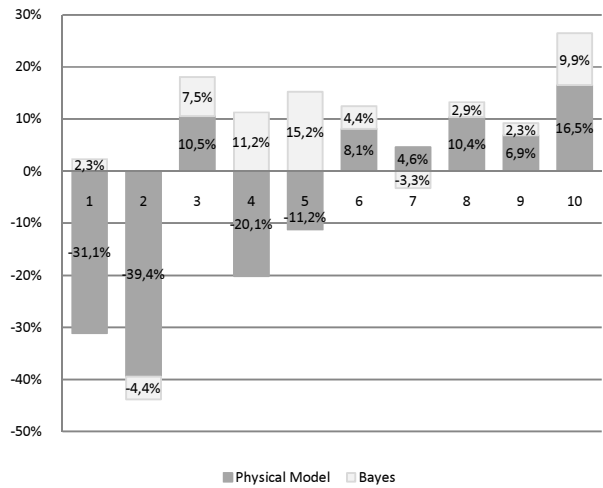


Figure 36 Percentage prediction error @ 75% FT

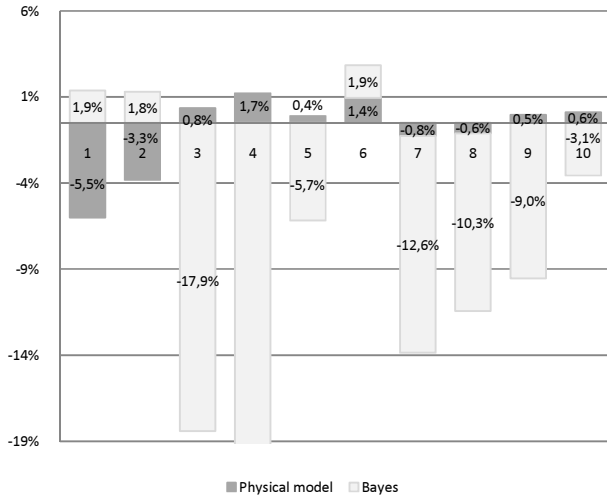


Figure 37 Percentage prediction error @ 98% FT

% Life	Model	c_1	c_2	c_3	c_4	c_5
25	Physical model	-98,50%	-66,59%	-1,20%	-	-
	Bayes	44,95%	-3,96%	-4,85%	58,58%	62,57%
50	Physical model	-86,08%	-66,11%	-0,55%	-	-
	Bayes	19,36%	5,77%	4,00%	30,77%	35,70%
75	Physical model	-31,09%	-39,44%	10,52%	-	-
	Bayes	2,31%	-4,42%	7,53%	11,24%	15,22%
98	Physical model	-5,52%	-3,31%	0,84%	1,72%	0,39%
	Bayes	1,87%	1,81%	-	-	-5,68%
% Life	Model	c_6	c_7	c_8	c_9	c_10
25	Physical model	32,56%	27,98%	41,74%	28,29%	57,91%
	Bayes	25,64%	39,37%	40,14%	41,39%	31,19%
50	Physical model	18,24%	11,76%	22,84%	12,63%	35,59%
	Bayes	15,11%	12,08%	12,15%	15,37%	19,54%
75	Physical model	8,09%	4,64%	10,39%	6,87%	16,52%
	Bayes	4,38%	-3,27%	2,87%	2,34%	9,91%
98	Physical model	1,44%	-0,76%	-0,61%	0,48%	0,61%
	Bayes	1,90%	-12,61%	-	-9,04%	-3,06%

Table 5 Percentage prediction errors

General considerations can be drafted from the conclusive graph in Figure 38 that displays the mean squared percentage error among the whole set for each residual life percentile. The statements of the list above are confirmed.

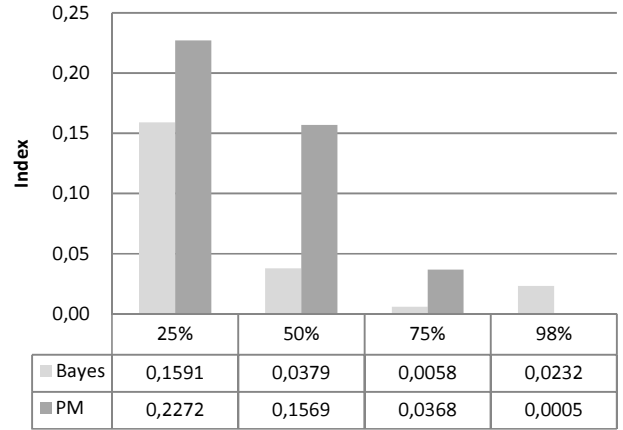


Figure 38 MS of the percentage prediction errors for each residual life percentile

Using the other metric chosen, expressed by Eq.3.2 the results displayed in Table 6 are obtained. The main difference between the metric defined before, is that this metric considers the whole set of predictions and not only those that corresponds to particular moments. The results found are very similar among the two approaches. The physical model index is slightly smaller than the Bayesian one.

	Physical model	Bayes	NDI - max	NDI - mean
c_1	1.07595	1.02061	34	33.24
c_2	1.05471	1.00486	40	39.49
c_3	1.00225	1.02235	47	42.41
c_4	1.02188	1.01337	61	58.98
c_5	1.01014	1.01547	71	68.61
c_6	1.00199	1.00774	75	73.04
c_7	1.00143	1.00769	86	82.14
c_8	1.00251	1.00787	100	96.19
c_9	1.00163	1.00240	105	100.35
c_10	1.00355	1.00484	115	110.70
MS	1.01791	1.01074		

Table 6 Results – φ , N_{insp} and \bar{N}_{insp}

The last two columns of Table 6 reports respectively the maximum non destructive inspections number and the expected NDI number. The last result is obtained multiplying the NDI cumulative number with the corresponding PC_{DET} .

Obviously, the expected NDI number increases as the FT increases. The NDI number that should be performed to guarantee a 99% chance to detect a crack before it reaches the length of 6cm is relevant. As a consequence, the availability of the asset is highly affected from this maintenance policy. The loose of availability and the numerous maintenance activities imply a considerable maintenance costs build up.

In Figure 39 the effect of an increase of the size error is displayed[§], considering the updating frequency of 90 km. Can be noticed that generally, as previously stated, the greater the size error, the lower the life exploited. However, the life exploited reduction is not relevant. An increase of 3 times of the size error causes a life exploited reduction of about 5% on average. For the figures in appendix can be noticed that the effect of the updating frequency is lower with respect to the error size effect.

The scarce effect of this important variables to the exploited life is due to the fact that an increase of the size error cause a reduction of the threshold a_{th} that however corresponds to a negligible life loss reduction thanks to the high crack growth rate that characterize the last part of the degradation phase. Greater effects shall be noticed when the size error is large enough to force the threshold a_{th} to be set at crack sizes at which the growth rate is lower (i.e at the end of the first degradation phase).

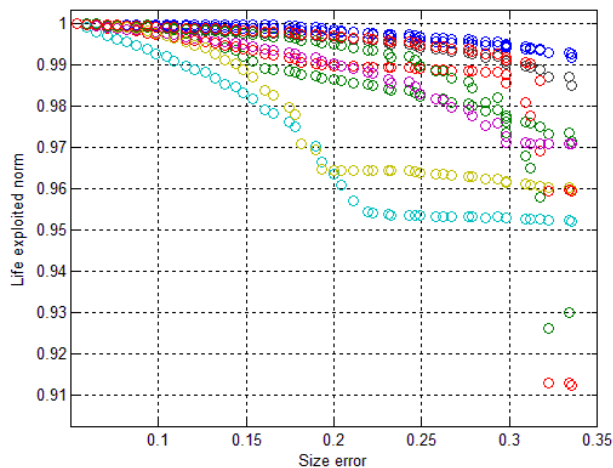


Figure 39 The size error effect on life exploited given $\delta = 90 \text{ km}^{**}$

[§] Computed considering the physical model predictions only

^{**} Life exploited is normalized with respect to the life exploited that corresponds to the first size error considered

4. CONCLUSIONS

The objective of this research was to propose an approach to a condition based maintenance policy assessment in order to preliminary evaluate its benefits and to understand the main variables that influence the overall approach performance. Particularly, an explanatory study was carried out to evaluate the possibility to introduce prognostic concepts into railway axle maintenance management.

Through a reliable probabilistic crack growth model a comparison between a prognostic maintenance approach based on Bayesian probabilistic theory, a prognostic maintenance approach based on the same crack growth physical model and the classical preventive maintenance policy based on regular NDT was carried out. The probabilistic crack growth model considers the SIF as a random normal variable and a random load history derived from measured load spectra. The diagnostic-monitoring infrastructure precision was described by a size error, directly derived from the calibration curve of an ultrasonic NDT. Assuming the hypothesis introduced in paragraph 2.3.4, the results suggests that further research should be conducted validating the approach proposed on a real case study. As matter of facts both the prognostic algorithms described guarantee an average absolute predictions errors lower than 50 % at 25% of the actual axle life. The later predictions guarantees lower prediction errors, approaching the 7% on average. Earlier predictions errors are generally lower for the Bayesian prognostic algorithm than those computed through the physical model. Whereas, for later predictions the physical model seem to provide more accurate RUL estimations. However, the gap between predictions error computed by the two models are, on average, comparable. The effect of the updating frequency and the size error on predictions errors in case of prognostic physical model algorithm scenario and therefore, on the overall approach performance (life exploited with a determined reliability threshold) is assessed as well. The results show that the higher the size error and the lower updating frequency the lower life exploited. However the effect of updating frequency and size error in terms of life exploited is limited till the maximum crack size threshold, derived from the error size of the diagnostic infrastructure, becomes lower than about 5 mm, i.e the crack size at which the crack growth rate significantly increases.

Generally speaking, a PHM approach needs a deep system/component knowledge. This need implies high investment costs to perform experimental tests (high fixed costs). System/component knowledge in high safety requirement environments, such as in the aviation industry, has to be known before commissioning for obvious safety reasons. Low Accuracy PHM May Be Worse Than No PHM. Costs and the benefits resulting from a prognostic approach could be distributed differently across the actors involved, therefore an “integrator” that manages all the

process is suggested or partnership between the main actors involved committed to share the investment costs. Moreover it is worth noting that a trade off exists between system usage pattern and the resulting benefits, higher usage allows a better return on investment but lowers t_{ADV} , i.e the main prognostic benefits driver.

After all these considerations, it is possible to sum up the results in the matrix displayed in Figure 40. Profitability of a PHM approach can be thought as a function of two variables:

- Component criticality
- Easiness to acquire data of component's failure modes

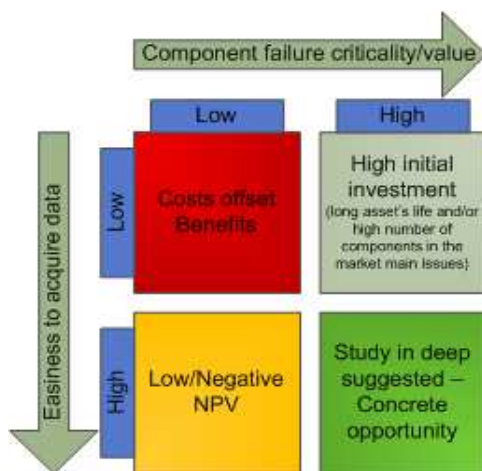


Figure 40: PHM applicability

Difficulties to describe and acquire data on the component's failure behavior imply high R&D costs while the components criticality and value can boost the benefits allowed by a PHM approach. The case in which a PHM approach is suggested is the case in which it is easy to acquire and data and knowledge on the component failure behavior and in which the component monitored and maintained is critical for the whole system availability and/or it has a very high value. In the other two situations further investigation aimed to better estimate the costs and the benefits involved is suggested.

ACKNOWLEDGEMENT

The author wishes to thank professors S.Beretta of the Polytechnic Institute of Milan (Italy) and G.Jacazio of the Polytechnic Institute of Turin (Italy) for their encouragement and support in the preparation of the paper

M.Vismara, Milan, 09/09/1985. Bachelor degree in Transport Engineering at Polytechnic of Milan. Master

degree in Mechanical Engineering at Polytechnic of Milan and Turin, ASP diploma (High Polytechnic School).

Maintenance Engineer at Hupac SA in Chiasso, Switzerland

REFERENCES

A.K Sheikh, M. A. (1983). Renewal Analysis Using Bernstein Distribution. *Reliability Engineering*, 5, 1-19.

A.Saxena, J. C. (2008). Metrics for Evaluating Performance of Prognostic Techniques. *International Conference on prognostics and health management*, (pp. 1-17). Denver, CO.

Anonymus. (2006). Fracture Mechanics and Fatigue Crack Growth 4.2. *NASA Technical report*.

C.J. Lu, W. M. (1993). Using Degradation Measures to Estimate a Time-to-Failure Distribution. *American Society for Quality*, 35 (2), 161-174.

C.P. Lonsdale, D. S. (2004). North american axle failure experience. *Proceedings of the Institution of Mechanical Engineers, Part F: Journal of Rail and Rapid Transit*, 218 (4), 293-298.

D. V. Lindley, A. F. (1972). Bayes estimates for the linear model. *Journal of the Royal Statistical Society, Series B, Statistical*, 34 (1), 1-41.

D.A. Virkler, B. H. (1979). The statistical nature of fatigue crack propagation. *ASME, Transactions, Journal of Engineering Materials and Technology*, 101, 148-153.

EN13103. (2001). *Railway applications - wheelsets and bogies - non powered axles - design method*.

Gassner, E. (1956). Performance fatigue testing with respect to aircraft design. In E. Gassner, *Fatigue in Aircraft Structures*. New York: Academic Press.

Hoddinot, D. (2004). Railway axle failure investigations and fatigue crack growth monitoring of an axle. *Proceedings of the Institution of Mechanical Engineers, Part F: Journal of Rail and Rapid Transit*, 218, 283-292.

J.L Bogdanoff, F. K. (1985). *Probabilistic models of cumulative damage*. New York: John Wiley & Sons.

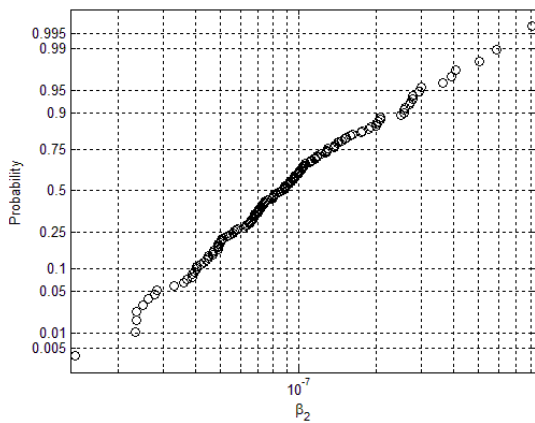
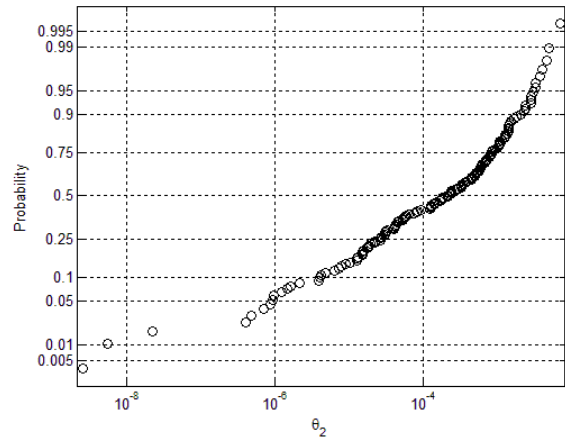
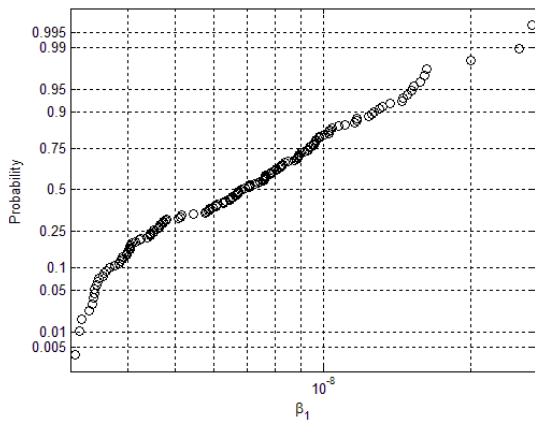
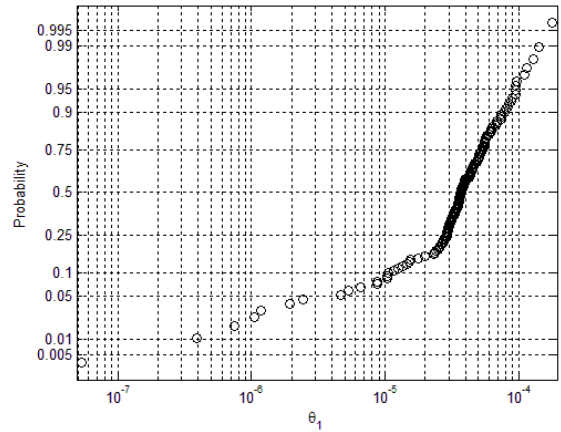
- K.Ortiza, A. (1988). Stochastic modeling of fatigue crack growth. *Engineering Fracture Mechanics* , 29 (3), 317-334.
- M. Carboni, S. B. (2007). Effect of probability of detection upon the definition of inspection intervals for railway axles. *Proceedings of the Institution of Mechanical Engineers, Part F: Journal of Rail and Rapid Transit* , 221 (3), 409-417.
- N. Gebraeel, J. P. (2008). Prognostic Degradation Models for Computing and Updating Residual Life Distributions in a Time-Varying Environment. *IEEE Transaction on Reliability* , 57 (4), 539-549.
- N. Gebraeel, M. L. (2005). Life distributions from component degradation signals: A Bayesian approach. *IIE Trans.* , 37 (6), 543–557.
- N.Z Gebraeel, K. K. (2009). Predictive Maintenance Management Using Sensor-Based Degradation Models. *IEEE Transactions on Systems, Man, and Cybernetics, Part A: Systems and Humans* , 39 (4), 840-849.
- R.A. Smith, S. (2004). A brief historical overview of the fatigue of railway axles. *Proceedings of the Institution of Mechanical Engineers, Part F: Journal of Rail and Rapid Transit* , 218 (4), 267-277.
- S. Beretta, M. C. (2004). Application of fatigue crack growth algorithms to railway axles and comparison of two steel grades. *Proceedings of the Institution of Mechanical Engineers, Part F: Journal of Rail and Rapid Transit* , 218 (4).
- S. Beretta, M. C. (2006). Experiments and stochastic model for propagation lifetime of railway axles. *Engineering Fracture Mechanics* , 73, 2627–2641.
- S.Beretta, M. M. (2006). SIF solutions for cracks at notches under rotating bending. *Proceedings of the 16th European Conference on Fracture (ECF16)*. Alexandropoulos.
- S.Beretta, M. (2005). Rotating vs. plane bending for crack growth in railway axles. *ESIS-TC24 Meeting*. Geesthacht.
- S.Beretta, M. (2005). Simulation of fatigue crack propagation in railway axles. *J ASTM Int* , 2 (5), 1-14.
- Schijve, J. (2001). *Fatigue of structures and materials*. Dordrecht: Kluwer Academic Publishers.
- U. Zerbst, K. M. (2005). Fracture mechanics in railway applications—an overview. *Engineering Fracture Mechanics* , 72, 163–194.
- U. Zerbst, M. V. (2005). The development of a damage tolerance concept for railway components and its demonstration for a railway axle. *Engineering Fracture Mechanics* , 72, 209–239.

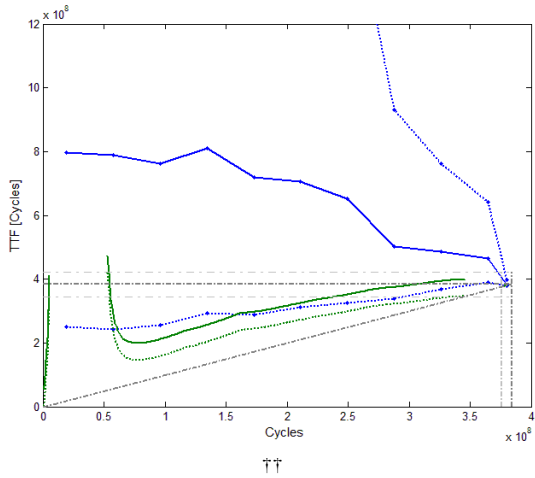
APPENDIX

In this paragraph graphs related to the first simulated crack growth path. They represent respectively:

- The predictions (lower bound, median and upper bound) on the TTF for
 - the prognostic physical model (blu lines)
 - the bayesian model (green lines)
- The probability of detection at each inspection
- The effect of the updating interval in km and the size error on the % of life exploited (physical model only)

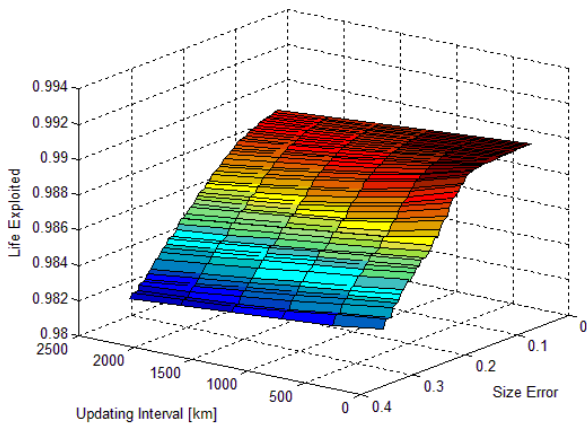
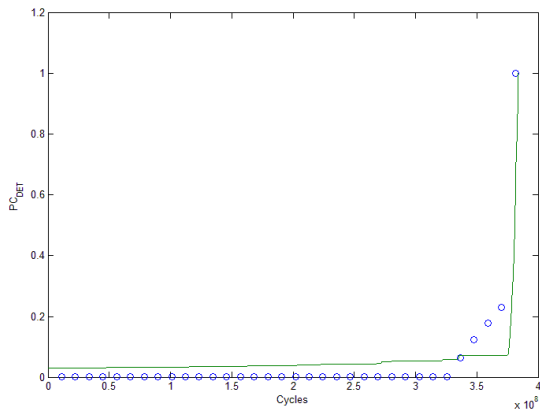
The first four probability plots represent the coefficients of the two exponential models used in the bayesian prognostic model.





DATA

- $\Delta K_{th} = N(11.32, 0.857) \text{ MPa}\sqrt{\text{m}}$ $n = 1.9966$
- $\Delta K_{th0} = 5.96 \text{ MPa}\sqrt{\text{m}}$ $C_{th} = -0.02$
- $R = -1$ $\alpha_1 = -194.024$
- $\Delta K_{crit} = 24 \text{ MPa}\sqrt{\text{m}}$ $\alpha_2 = 322.544$
- $p = 1.3$ $\alpha_3 = -177.24$
- $q = 0.001$ $\alpha_4 = 41.957$
- $\alpha_5 = -1.916$ $D = 160 \text{ mm}$
- $\alpha_6 = -0.3927$ $K_t = 1.2$
- $\beta = 0.656$
- $\varepsilon = 10 \text{ MPa}$
- $\vartheta = 2.5$
- $S_0 = 0.2$



†† Blue line: Physical model TTF estimation with confidence bounds (dotted)
 Green Line: Bayesian model TTF estimations with lower confidence bound (dotted)